AD-A041 058 COMPUTER CODE CONSULTANTS SOLANA BEACH CALIF F/G 19/4
THREE-DIMENSIONAL COMPUTATIONS ON PENETRATOR-TARGET INTERACTION--ETC(U)
APR 77 W E JOHNSON DAAD05-75-C-0738

UNCLASSIFIED BRL-CR-338 NL

1 OF 1
ADA
041058

END

DATE
FILMED
7-77

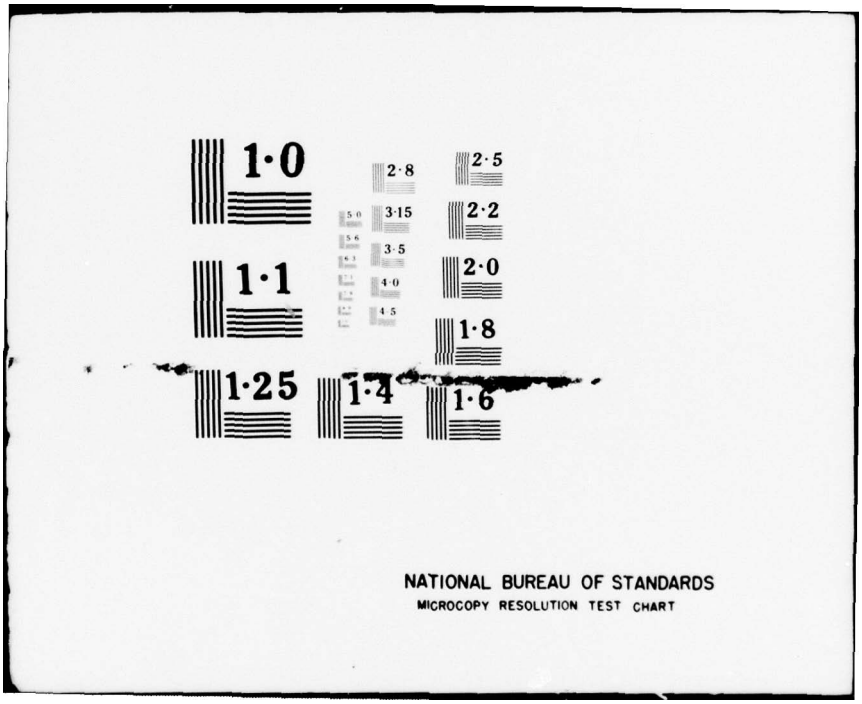
1·0
1·1
1·25
1·4
1·6
1·8
2·0
2·2
2·5
2·8
3·15
3·5
4·0
4·5
5·0
5·6
6·3
NATIONAL BUREAU OF STANDARDS
MICROCOPY RESOLUTION TEST CHART

AD A041058

BRL CR 338

BRL

12

AD

CONTRACT REPORT NO. 338

THREE-DIMENSIONAL COMPUTATIONS ON PENETRATOR-TARGET INTERACTIONS

Prepared by

Computer Code Consultants
527 Glencrest Drive
Solana Beach, CA 92075

DDC
RECEIVED
JUN 29 1977
C

April 1977

ORIGINAL CONTAINS COLOR PLATES: ALL DDC REPRODUCTIONS WILL BE IN BLACK AND WHITE.

Approved for public release; distribution unlimited.

USA ARMAMENT RESEARCH AND DEVELOPMENT COMMAND
USA BALLISTIC RESEARCH LABORATORY
ABERDEEN PROVING GROUND, MARYLAND

AD No.
DDC FILE COPY

Destroy this report when it is no longer needed.
Do not return it to the originator.

Secondary distribution of this report by originating or sponsoring activity is prohibited.

Additional copies of this report may be obtained from the National Technical Information Service, U.S. Department of Commerce, Springfield, Virginia 22151.

The findings in this report are not to be construed as an official Department of the Army position, unless so designated by other authorized documents.

UNCLASSIFIED
SECURITY CLASSIFICATION OF THIS PAGE *(When Data Entered)*

REPORT DOCUMENTATION PAGE	READ INSTRUCTIONS BEFORE COMPLETING FORM
1. REPORT NUMBER: BRL Contract Report No. 338	2. GOVT ACCESSION NO.: CR-338
3. RECIPIENT'S CATALOG NUMBER:	
4. TITLE *(and Subtitle)*: Three-Dimensional Computations on Penetrator-Target Interactions	5. TYPE OF REPORT & PERIOD COVERED: BRL Contractor Report, Nov 1974 - Dec 1975
	6. PERFORMING ORG. REPORT NUMBER:
7. AUTHOR(s): Wallace E. Johnson	8. CONTRACT OR GRANT NUMBER(s): DAAD05-75-C-0738
9. PERFORMING ORGANIZATION NAME AND ADDRESS: Computer Code Consultants, 527 Glencrest Drive, Solana Beach, California 92075	10. PROGRAM ELEMENT, PROJECT, TASK AREA & WORK UNIT NUMBERS: 61102A, 1T161102A33, 002AJ
11. CONTROLLING OFFICE NAME AND ADDRESS: USA Ballistic Research Laboratory, Aberdeen Proving Ground, Maryland 21005	12. REPORT DATE: APR 1977
	13. NUMBER OF PAGES: 62
14. MONITORING AGENCY NAME & ADDRESS *(if different from Controlling Office)*: 54 p.	15. SECURITY CLASS. *(of this report)*: Unclassified
	15a. DECLASSIFICATION/DOWNGRADING SCHEDULE:

16. DISTRIBUTION STATEMENT *(of this Report)*

Approved for public release; distribution unlimited.

17. DISTRIBUTION STATEMENT *(of the abstract entered in Block 20, if different from Report)*

18. SUPPLEMENTARY NOTES

19. KEY WORDS *(Continue on reverse side if necessary and identify by block number)*

Jet Penetration
Hypervelocity Impact
Hydrodynamic Code
Eulerian Code
Two-dimensional Code
Impact Mechanics
Shaped Charge Jets
Fuel Impact

20. ABSTRACT *(Continue on reverse side if necessary and identify by block number)*

The three-dimensional, two-material, rigid-plastic code, TRIDORF, was used to solve penetration calculations of shaped charge jets impacting thin targets at four angles of obliquity. A fuel target interaction with a shaped charge jet was solved by using the two-dimensional DORF code and the TRIDORF code.

DD FORM 1 JAN 73 1473 EDITION OF 1 NOV 65 IS OBSOLETE

UNCLASSIFIED
SECURITY CLASSIFICATION OF THIS PAGE *(When Data Entered)*

TABLE OF CONTENTS

		Page
	LIST OF ILLUSTRATIONS	v
I.	INTRODUCTION	1
II.	DESCRIPTION OF NUMERICAL TECHNIQUE	2
	A. Difference Equations for Phase 1	3
	B. Difference Equations for Phase 2	11
	C. Difference Equations for Phase 3	15
III.	TWO-DIMENSIONAL, THREE-DIMENSIONAL COMPARISON	23
IV.	OBLIQUE IMPACTS	23
V.	FUEL TARGET INTERACTION	24
VI.	MULTI-MATERIAL IMPACT	26
VII.	CODE MODIFICATIONS	27
	ACKNOWLEDGEMENTS	28
	FIGURES	29
	DISTRIBUTION LIST	61

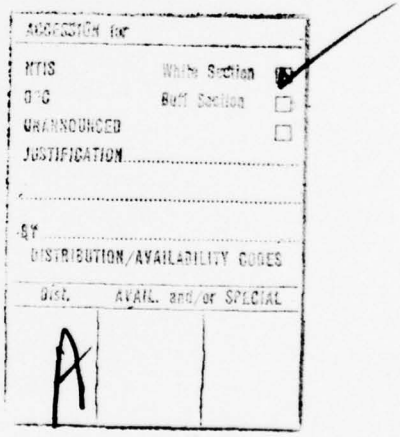

PRECEDING PAGE BLANK-NOT FILMED

LIST OF ILLUSTRATIONS

Figure		Page
III-1.	2D-3D Initial Configuration for Normal Impact	29
III-2.	Pressure Versus Distance (into Target) for 2D - 3D	30
IV-1.	Density as a Function of Time for the Normal Impact	31
IV-1.	Density as a Function of Time for the Normal Impact (continued)	32
IV-2.	Density as a Function of Time for the 45° Impact	33
IV-2.	Density as a Function of Time for the 45° Impact (continued)	34
IV-3.	Density as a Function of Z at a Time of 3.57μsec for the 30° Impact	35
IV-3.	Density as a Function of Z at a Time of 3.57μsec for the 30° Impact (continued)	37
IV-4.	Density as a Function of Z at a Time of 4.41μsec for the 45° Impact	39
IV-4.	Density as a Function of Z at a Time of 4.41μsec for the 45° Impact (continued)	41
IV-5.	Density as a Function of Time and Z for the 60° Impact	43
IV-5.	Density as a Function of Time and Z for the 60° Impact (continued)	45
IV-6.	Density as a Function of Z for the 77.5° Impact	47
IV-6.	Density as a Function of Z for the 77.5° Impact (continued)	49

PRECEDING PAGE BLANK-NOT FILMED

LIST OF ILLUSTRATIONS (Continued)

Figure		Page
V-1.	Initial Fuel Target Interaction (2D - 3D)	51
V-2.	Pressures in 3D Mesh at Time of Rezone	52
V-3.	Pressure Contours at Completion of 3D Calculations	53
V-4.	Pressure Distribution at Completion of 3D Calculation	55
VI-1.	Initial Configuration for the Multi-Material Normal Impact	56
VI-2.	Density as a Function of Time for the Multi-Material Normal Impact	57
VI-2.	Density as a Function of Time for the Multi-Material Normal Impact (continued)	59

I. INTRODUCTION

For several years the Ballistics Research Laboratories, using computer codes, have been investigating the phenomena associated with the penetration by a shaped-charged jet into vehicle armor. The purpose of these investigations has been to provide an armor configuration that is light in weight but effective against shaped-charged jets.

The computer codes presently available can numerically solve problems of normal or zero obliquity impact. For plane strain, planes of non-zero obliquity can be solved using X-Y versions of Eulerian codes. There are certain unique phenomena which occur during oblique impact; consequently, a three-dimensional model of the penetration process is required to investigate in detail the phenomena associated with oblique impact.

TRIDORF[2] is capable of performing these oblique impact calculations. TRIDORF is a two-material version of TRIOIL[1] with a rigid-perfectly plastic strength formulation. The description of the TRIDORF code is reported in Section II. A normal impact has been checked against the DORF[3] code (two-dimensional) and is reported in Section III.

A series of four oblique impact calculations (copper jet impacting a steel plate) have been solved using the TRIDORF code and are reported in Section IV. In addition, three oblique impact calculations (plexiglass spheres impacting a plexiglass plate) performed for the Naval Research Laboratory are reported in Section IV.

A fuel target configuration has been calculated with a two-dimensional model (DORF) transferring over to the three-dimensional model (TRIDORF) when the stress wave (generated by the rigid jet) reaches the walls of the cylinder.

---

[1] Johnson, W. E., "TRIOIL - A Three-Dimensional Version of the OIL Code," GAMD-7310, General Atomic, June 1967.

[2] Johnson, W. E., "TRIDORF - A Two-Material Version of the TRIOIL Code with Strength," Computer Code Consultants, to be published.

[3] Johnson W. E., "Code Correlation Study," Technical Report No. AFWL-TR-70-144, April 1971; and Johnson, W. E., "Development and Application of Computer Programs to Hypervelocity Impact," 3SR-749, Systems, Science and Software, July 1971.

The results of these calculations are described in Section V. The code modifications, for both DORF and TRIDORF, required for these tasks are described in Section VII.

A multi-material normal impact calculation has been solved using the DORF[3] code and is reported in Section VI. A splitting (a method of fractional steps, where one can replace a complicated multi-dimensional problem by a succession of simpler one-dimensional ones) version of the OIL[4] code and techniques to eliminate the conventional "if" tests from Eulerian formulations are described in Section VII.

II. DESCRIPTION OF NUMERICAL TECHNIQUES

The TRIOIL[1] code has been modified to treat two materials, and a rigid-perfectly plastic strength model has been included. A routine to move massless tracer particles has also been incorporated into the code. This version is called TRIDORF[2] and is in the final state of documentation. The basic difference equations for the Lagrangian phase, the convective phase and the strength phase are listed below. Familiarity with the OIL[4] family of codes is assumed.

---

[4]Johnson, W. E., "OIL - A Continuous Two-Dimensional Eulerian Hydrodynamic Code," GAMD-5580, General Atomic, June 1965.

A. Difference Equations For Phase 1 (Lagrangian Phase)

The Eulerian equations we wish to solve are the following:

$$\frac{\partial \rho}{\partial t} + \nabla \cdot (\rho \vec{u}) = 0 \qquad (1)$$

$$\frac{\partial \rho \vec{u}}{\partial t} + \vec{u} \cdot \nabla \rho \vec{u} = -\nabla P \qquad (2)$$

$$\frac{\partial \rho E}{\partial t} + \nabla \cdot (\rho E \vec{u}) = -\nabla \cdot (P \vec{u}) \qquad (3)$$

Equation 1 is the conservation of mass equation, Equation 2 is the conservation of momentum equation, and Equation 3 is the conservation of energy equation.

The second terms on the left side of Equations 1, 2 and 3 are temporarily dropped. Their contributions are later approximated when we move mass across cell boundaries. Rewriting Equations 2 and 3 in cartesian coordinates results in Equations 4, 5, 6 and 7.

$$\rho \frac{\partial u}{\partial t} = - \frac{\partial P}{\partial x} \qquad (4)$$

$$\rho \frac{\partial v}{\partial t} = - \frac{\partial P}{\partial y} \qquad (5)$$

$$\rho \frac{\partial w}{\partial t} = - \frac{\partial P}{\partial z} \qquad (6)$$

$$\rho \frac{\partial E}{\partial t} = - \frac{\partial (Pu)}{\partial x} - \frac{\partial (Pv)}{\partial y} - \frac{\partial (Pw)}{\partial z} \qquad (7)$$

ρ = density of cell L, g/cm^3

x = x coordinate, cm

y = y coordinate, cm

z = z coordinate, cm

u = x component of velocity, cm/shake
(1 shake = 10^{-8} sec)

v = y component of velocity, cm/shake

w = z component of velocity, cm/shake

P = $f(\rho,Q)$ from the equation of state
= material pressure, $jerks/cm^3$
(1 jerk = 10^{16} ergs)

E = total specific energy, jerks/g

t = time, shakes

Q = specific internal energy, jerks/g.

Rewriting Equation 7,

$$\rho \frac{\partial E}{\partial t} = - \frac{\partial (Pu)}{\partial x} - \frac{\partial (Pv)}{\partial y} - \frac{\partial (Pw)}{\partial z}$$

or, substituting for the total specific energy,

$$\rho \frac{\partial}{\partial t} \left[Q + \frac{1}{2} \left(u^2 + v^2 + w^2 \right) \right] = - \frac{\partial (Pu)}{\partial x} - \frac{\partial (Pv)}{\partial y} - \frac{\partial (Pw)}{\partial z}$$

and differentiating ,

$$\rho \frac{\partial Q}{\partial t} + \rho u \frac{\partial u}{\partial t} + \rho v \frac{\partial v}{\partial t} + \rho w \frac{\partial w}{\partial t} = -P \frac{\partial u}{\partial x} - u \frac{\partial P}{\partial x}$$

$$- P \frac{\partial v}{\partial y} - v \frac{\partial P}{\partial y} - P \frac{\partial w}{\partial z} - w \frac{\partial P}{\partial z} ,$$

But

$$\rho \frac{\partial u}{\partial t} = - \frac{\partial P}{\partial x} \quad \text{and} \quad \rho \frac{\partial v}{\partial t} = - \frac{\partial P}{\partial y} \quad \text{and} \quad \rho \frac{\partial w}{\partial t} = - \frac{\partial P}{\partial z},$$

thus

$$\rho \frac{\partial Q}{\partial t} = -P \left[\frac{\partial u}{\partial x} + \frac{\partial v}{\partial y} + \frac{\partial w}{\partial z} \right] . \qquad (8)$$

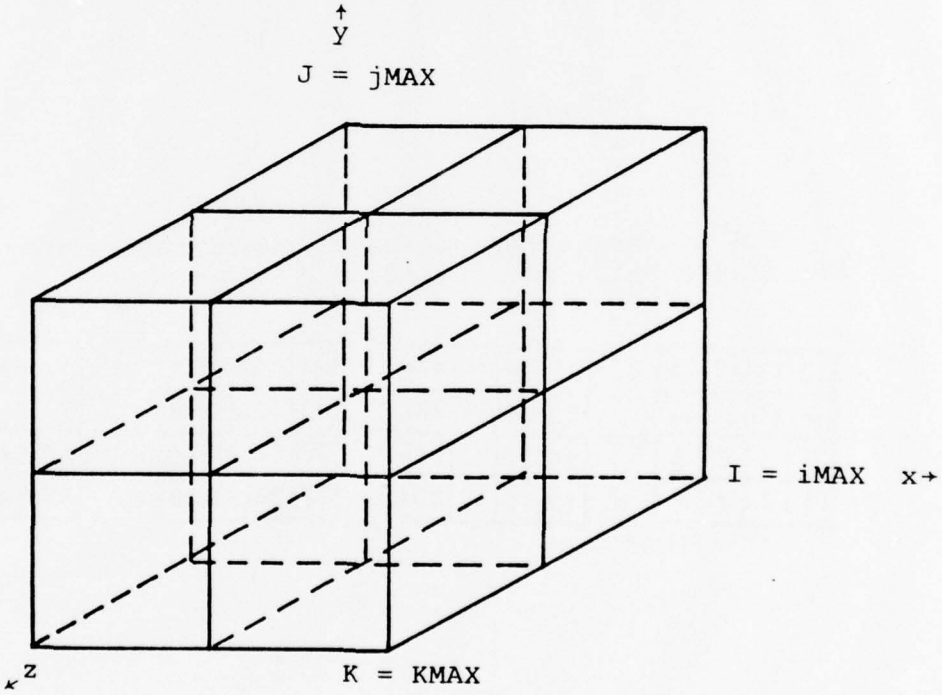

A VIEW OF A THREE-DIMENSIONAL GRID

The ρ, u, v, w, P, E and Q are all cell-centered quantities with the cell index L, which is defined as

$$L = (J-1)\ iMAX + I + (K-1)\ iXMAX$$

where $iXMAX = (iMAX)(jMAX)$.

Also,

$$x(I) = \sum_{i=1}^{I} \Delta x(i)$$

$$y(J) = \sum_{j=1}^{J} \Delta y(j)$$

$$z(K) = \sum_{k=1}^{K} \Delta Z(k) \quad .$$

The L storage for the cell quantities is indicated in the figure below for a grid of $4 \times 4 \times 4$.

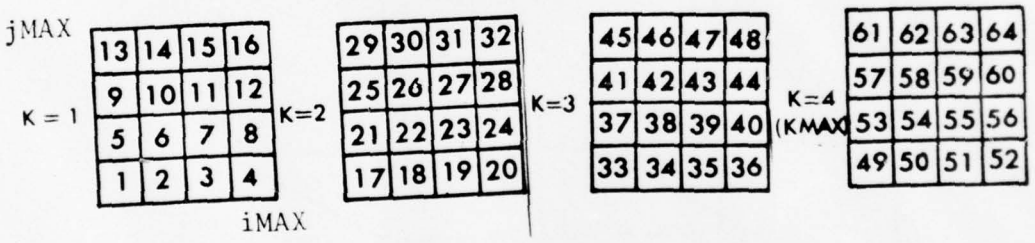

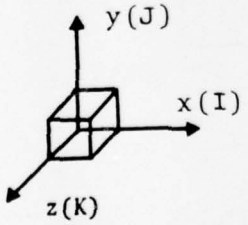

The x-momentum equation (4) becomes, in difference form,

$$\rho_L^n\left(\frac{\tilde{u}_L - u_L^n}{\Delta t}\right) = \frac{P_{L-1}^n - P_{L+1}^n}{2\Delta x(I)} \quad .$$

The y-momentum equation (5) becomes, in difference form,

$$\rho_L^n\left(\frac{\tilde{v}_L - v_L^n}{\Delta t}\right) = \frac{P_{L-iMAX}^n - P_{L+iMAX}^n}{2\Delta y(J)} \; .$$

The z-momentum equation (6) becomes, in difference form,

$$\rho_L^n\left(\frac{\tilde{w}_L - w_L^n}{\Delta t}\right) = \frac{P_{L-iXMAX}^n - P_{L+iXMAX}^n}{2\Delta z(K)} \; .$$

The ($\tilde{}$) refers to the velocities at the completion of Phase 1 (not at cycle n+1, since we have neglected the transport terms at this stage). Here the acceleration of cell L is seen to depend only on the pressures in the neighboring cells and not that of L. Defining pressures at interfaces,

$$PL^n = \frac{P_{L-1}^n + P_L^n}{2} \qquad PBLO^n = \frac{P_{L-iMAX}^n + P_L^n}{2}$$

$$PRR^n = \frac{P_L^n + P_{L+1}^n}{2} \qquad PABOVE^n = \frac{P_L^n + P_{L+iMAX}^n}{2}$$

$$PBIND^n = \frac{P^n_{L-iXMAX} + P^n_L}{2}$$

$$PZR^n = \frac{P^n_{L+iXMAX} + P^n_L}{2} \quad .$$

Substitution of these interface pressures into the three-momentum equations results in

$$\tilde{u}_L - u^n_L = \frac{\Delta t}{\rho^n_L}\left[\frac{PL^n - PRR^n}{\Delta x(I)}\right]$$

$$\tilde{v}_L - v^n_L = \frac{\Delta t}{\rho^n_L}\left[\frac{PBLO^n - PABOVE^n}{\Delta y(J)}\right]$$

$$\tilde{w}_L - w^n_L = \frac{\Delta t}{\rho^n_L}\left[\frac{PBIND^n - PZR^n}{\Delta z(K)}\right]$$

where the usual tilda (~) designates the new velocities (not at cycle n+1), since we have temporarily dropped the transport terms.

The specific internal energy equation becomes

$$\frac{\Delta Q}{\Delta t} = -p^n_L\left[\frac{v^{n+1/2}_{L-iMAX} - v^{n+1/2}_{L+iMAX}}{2\Delta y(J)} + \frac{u^{n+1/2}_{L-1} - u^{n+1/2}_{L+1}}{2\Delta x(I)}\right.$$

$$\left. + \frac{w^{n+1/2}_{L-iXMAX} - w^{n+1/2}_{L+iXMAX}}{2\Delta z(K)}\right] \Big/ MASS$$

$$MASS = AMX(L) + AMD(L)$$

where Q = specific internal energy, AMX = X mass of cell, gm and AMD = · mass of cell, gm. The reason for the velocities at time (n+1/2) can be seen from energy conservation considerations. Defining

$$u_L^{n+1/2} = \frac{u_L^n + \tilde{u}_L}{2}$$

$$v_L^{n+1/2} = \frac{v_L^n + \tilde{v}_L}{2}$$

$$w_L^{n+1/2} = \frac{w_L^n + \tilde{w}_L}{2}$$

and

$$VBLO = \frac{v_L + v_{L-iMAX}}{2}$$

$$VABOVE = \frac{v_L + v_{L+iMAX}}{2}$$

$$UL = \frac{U_L + U_{L-1}}{2}$$

$$URR = \frac{U_L + U_{L+1}}{2}$$

$$UBIND = \frac{W_L + W_{L-iXMAX}}{2}$$

$$WZR = \frac{W_L + W_{L+iXMAX}}{2}$$

then

$$\left(\frac{\Delta Q}{\Delta t}\right) = P_L^n \left[\frac{VBLO^n + \tilde{VBLO}}{2\Delta y(J)} - \frac{VABOVE^n + \tilde{VABOVE}}{2\Delta y(J)} + \frac{UL^n + \tilde{UL}}{2\Delta x(I)} \right.$$

$$\left. - \frac{URR^n + \tilde{URR}}{2\Delta x(I)} + \frac{UBIND^n + \tilde{UBIND}}{2\Delta z(K)} - \frac{WZR^n + \tilde{WZR}}{2\Delta z(K)} \right] \Big/ MASS$$

The solution of the momentum equations are very straightforward; however, the solution to the energy equation requires the old and new velocities. Two passes are made through the routine: The first pass formulates the interface velocities for the work term contribution to the internal energy before integrating the momentum equations (since we have allowed only one array per velocity component), and the second pass bypasses the momentum equations and only computes the new interface velocities for their contribution to the work term.

The change in specific internal energy for each material is assumed to be proportional to the fractional volume of each

$$\Delta Q_x = \Delta Q f / M_x$$

and

$$\Delta Q_\cdot = \Delta Q (1-f) / M_\cdot$$

where (x) and (·) refer to the two different materials, x and dot respectively, and f is the fraction of the total cell volume occupied by (x) material. The factor, f, is calculated from the equation of state, where we iterate on the densities until the pressures of each material are the same.

B. Difference Equations For Phase 2 (Convective Phase)

The Eulerian equations we wish to solve are the following:

$$\frac{\partial \rho}{\partial t} = -\nabla \cdot (\rho \vec{u}) \tag{9}$$

$$\frac{\partial \rho u}{\partial t} = -\vec{u} \cdot \nabla \rho \vec{u} \tag{10}$$

$$\frac{\partial \rho E}{\partial t} = -\nabla \cdot (\rho E \vec{u}) \tag{11}$$

Rewriting Equation 9, the mass transport equation in finite difference form results in

$$\frac{\rho_L^{n+1} - \rho_L^n}{\Delta t} = \left[\frac{\rho_{J-1}^n \bar{v}_{J-1} - \rho_J^n \bar{v}_J}{\Delta y(J)} + \frac{\rho_{I-1}^n \bar{u}_{I-1} - \rho_I \bar{u}_I}{\Delta x(I)} + \frac{\rho_{K-1}^n \bar{w}_{K-1} - \rho_K^n \bar{w}_K}{\Delta Z(K)} \right].$$

The velocities $\bar{v}$, $\bar{u}$ and $\bar{w}$ are average type velocities as described in Reference 1.

Mass, the three components of momentum and the energy across all six sides of the parallelpiped are calculated. By conserving the x, y and z momentum and the total energy, the new velocities are calculated and the new specific internal energy is the difference between the total energy in the cell (after transport) and the new kinetic energy.

For the mass fluxes, we must determine (for a mixed cell) how much of each material to move. Four possible situations concerned with two materials arise.

(1) Material moving from a non-mixed cell to a mixed cell. This presents no difficulty or modification to the transport terms.

EXAMPLE (non-mixed to mixed):

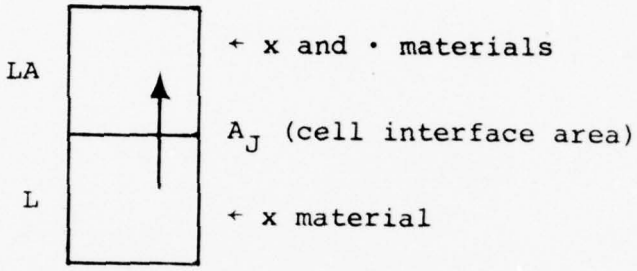

Mass flow is from cell L to cell LA.

$$\Delta M = \rho_L \bar{v} A_J \Delta t$$

$$\Delta M_x = \Delta M$$

$$\Delta M_\bullet = 0$$

where ρ = density of x material in cell L.

(2) From a mixed to a pure cell:

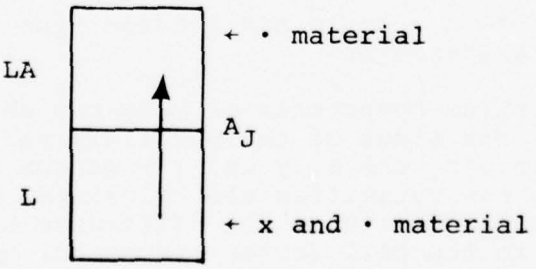

The flux is positive from cell L to cell LA.

The volume of material to move from cell L to cell LA is $\bar{V}\Delta t$ (DX(I) DZ(K)) where $\bar{V}$ is the weighted velocity to use in the mass flux equation. The volume of x material in cell L is VOL, the volume of the dot material is (1-f)VOL.

A. If $\bar{V}\Delta t$ (DX(I) DZ(K)) > (1-f)VOL, let all the dot mass move out, that is, set $\Delta M_{\cdot}$ = AMD(L). Now the remainder of the volume to move will be assigned to the x flux as follows: We can calculate the x mass to move from conservation of partial volumes,

$$\bar{V}\Delta t(DX(I)\ DZ(K)) = VOL_x + VOL_{\cdot} = \frac{\Delta M_x}{\rho_x} + (1-f)VOL_{\cdot}$$

But

$$\rho_x = \frac{AMX(L)}{f\ VOL} ,$$

thus

$$\Delta M_x = [\bar{V}\ \Delta t - (1-f)\ DY(J)]\ \frac{AMX(L)}{f\ DY(J)}$$

B. If $\bar{V}\Delta t$(DX(I) DZ(K)) < (1-f)VOL then the x mass to move ΔM_X is set to 0 and the dot mass to move $\Delta M_{\cdot}$ is given by

$$\Delta M_{\cdot} = \frac{AMD(L)}{(1-f)DY(J)}\ \bar{V}\ \Delta t = \rho\bar{V}\ A\Delta t\ .$$

(3) Material moving from a mixed cell to a mixed cell requires some modification in the transport terms in order to keep the material interface defined in a single mixed cell.

EXAMPLE (mixed to mixed):

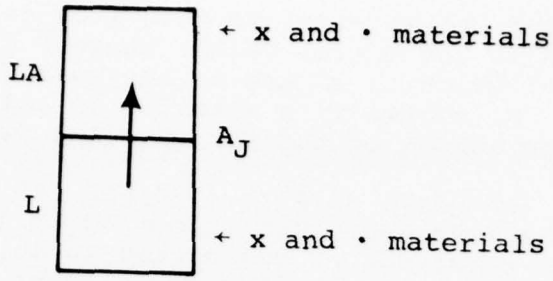

Mass flow is from cell L to cell LA. $\Delta M = \rho \overline{V} A_J \Delta t$, where ρ is the total density of both materials in cell L, then

$$\Delta M_x = \frac{M_x^L + M_x^{LA}}{M_x^L + M_x^{LA} + M_\cdot^L + M_\cdot^{LA}} \Delta M$$

$$\Delta M_\cdot = \frac{M_\cdot^L + M_\cdot^{LA}}{M_x^L + M_x^{LA} + M_\cdot^L + M_\cdot^{LA}} \Delta M$$

(4) From a mixed to a pure cell, with a pure like material below – use the mass weighting scheme as calculated in situation Number 3.

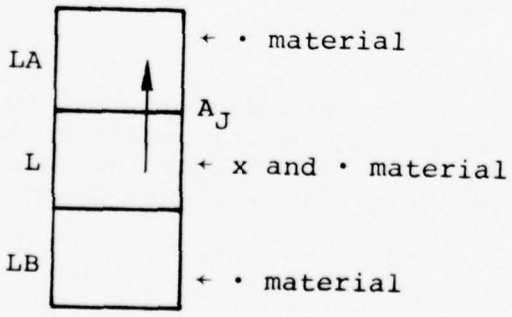

C. Difference Equations For Phase 3 (Strength Phase)

The Eulerian equations for the rigid-perfectly plastic strength equations are again, dropping the transport terms:

Conservation of Momentum:

$$\rho \frac{\partial u_i}{\partial t} = \sigma_{ij,j}$$

Conservation of Energy:

$$\rho \frac{\partial E}{\partial t} = (\sigma_{ij}\, u_i),\ j$$

where E = total energy per gram, internal plus kinetic.

The deviatoric stresses are defined as

$$\sigma_{ij} = B\left(\dot{e}_{ij} - \delta_{ij}\frac{\dot{e}_{aa}}{3}\right) = B\,\dot{\varepsilon}_{ij}$$

where

$$B = \frac{y\sqrt{2}}{\sqrt{\dot{\varepsilon}_{ab}\,\dot{\varepsilon}_{ab}}} \quad \text{(y is defined on page 22)}$$

$$\dot{e}_{ij} = \begin{Bmatrix} \frac{\partial u}{\partial x} & \frac{1}{2}\left(\frac{\partial u}{\partial y} + \frac{\partial v}{\partial x}\right) & \frac{1}{2}\left(\frac{\partial u}{\partial z} + \frac{\partial w}{\partial x}\right) \\ \frac{1}{2}\left(\frac{\partial v}{\partial x} + \frac{\partial u}{\partial y}\right) & \frac{\partial v}{\partial y} & \frac{1}{2}\left(\frac{\partial v}{\partial z} + \frac{\partial w}{\partial y}\right) \\ \frac{1}{2}\left(\frac{\partial w}{\partial x} + \frac{\partial u}{\partial z}\right) & \frac{1}{2}\left(\frac{\partial w}{\partial y} + \frac{\partial v}{\partial z}\right) & \frac{\partial w}{\partial z} \end{Bmatrix}$$

$$\dot{\varepsilon}_{ij}\,\dot{\varepsilon}_{ij} = \left(\dot{e}_{ij} - \frac{\delta_{ij}\,\dot{e}_{aa}}{3}\right)^2$$

$$= \left(\frac{\partial u}{\partial x}\right)^2 + \left(\frac{\partial v}{\partial y}\right)^2 + \left(\frac{\partial w}{\partial z}\right)^2 + 2\left[\frac{1}{2}\left(\frac{\partial v}{\partial x} + \frac{\partial u}{\partial y}\right)\right]^2$$

$$+ 2\left[\frac{1}{2}\left(\frac{\partial u}{\partial z} + \frac{\partial w}{\partial x}\right)\right]^2 + 2\left[\frac{1}{2}\left(\frac{\partial v}{\partial z} + \frac{\partial w}{\partial y}\right)\right]^2$$

$$- \frac{1}{3}\left(\frac{\partial u}{\partial x} + \frac{\partial v}{\partial y} + \frac{\partial w}{\partial z}\right)^2$$

$$= \left(\frac{\partial u}{\partial x}\right)^2 + \left(\frac{\partial v}{\partial y}\right)^2 + \left(\frac{\partial w}{\partial z}\right)^2$$

$$- \frac{1}{3}\left[\frac{\partial u}{\partial x} + \frac{\partial v}{\partial y} + \frac{\partial w}{\partial z}\right]^2$$

$$+ \frac{1}{2}\left(\frac{\partial v}{\partial x} + \frac{\partial u}{\partial y}\right)^2 + \frac{1}{2}\left(\frac{\partial u}{\partial z} + \frac{\partial w}{\partial x}\right)^2 + \frac{1}{2}\left(\frac{\partial v}{\partial z} + \frac{\partial w}{\partial y}\right)^2$$

The forces these stresses produce are then simply the stresses multiplied by the area over which they are acting.

These stresses are indicated in the following figure.

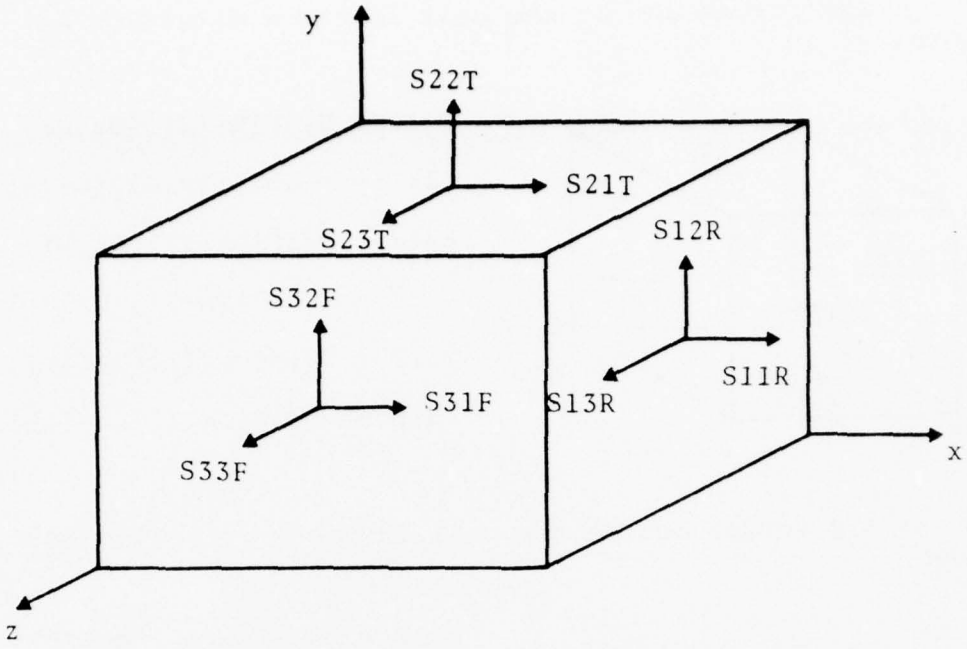

In addition to the nine stresses as shown, there are three on the left, three on the back and three on the bottom side of the cell, a total of 18 stresses.

There are six forces acting on the cell in the y direction as shown.

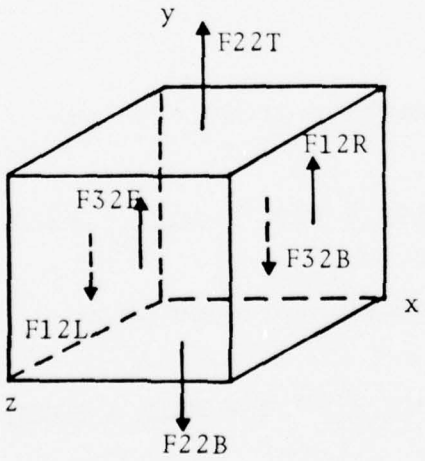

F22T = S22T(Dx(I))(Dz(K))

F22B = -S22B(Dx(I))(Dz(K))

F12R = S12R(Dy(J))(Dz(K))

F12L = -S12L(Dy(J))(Dz(K))

F32F = S32F(Dx(I))(Dy(J))

F32B = -S32B(Dx(I))(Dy(J))

Six forces act on the cell in the x direction as shown.

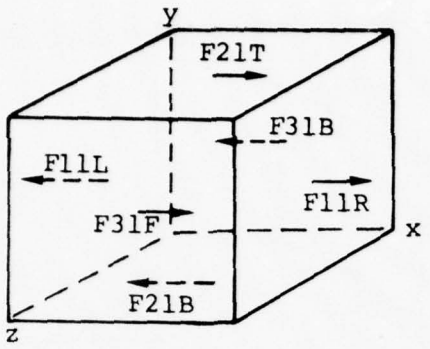

$$F11R = S11R(Dy(J))(Dz(K))$$

$$F11L = - S11L(Dy(J))(Dz(K))$$

$$F21T = S21T(Dx(I))(Dz(K))$$

$$F21B = -S21B(Dx(I))(Dz(K))$$

$$F31F = S31F(Dx(I))(Dy(J))$$

$$F31B = -S31B(Dx(I))(Dy(J))$$

Six forces act on the cell in the z direction as shown.

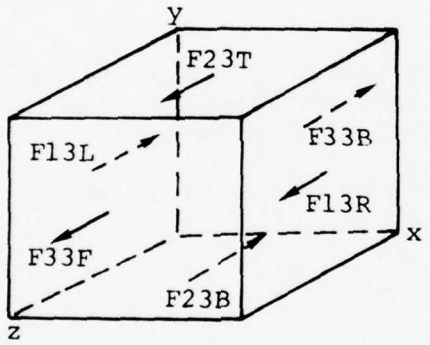

$$F33F = S33F(Dx(I))(Dy(J))$$

$$F33B = -S33B(Dx(I))(Dy(J))$$

$$F13R = S13R(Dy(J))(Dz(K))$$

$$F13L = -S13L(Dy(J))(Dz(K))$$

$$F23T = S23T(Dx(I))(Dz(K))$$

$$F23B = -S23B(Dx(I))(Dz(K))$$

The six forces in the z direction produce an acceleration of

$$\frac{dw}{dt} = \frac{1}{M_{(L)}} [F33F + F33B + F13R + R13L + F23T + F23B].$$

The six forces in the x direction produce an acceleration of

$$\frac{du}{dt} = \frac{1}{M_{(L)}} [F11R + F11L + F21T + F21B + F31F + F31B]$$

and the six forces in the y direction produce an acceleration of

$$\frac{dv}{dt} = \frac{1}{M_{(L)}} \left[F22T + F22B + F12R + F12L + F32F + F32B\right] .$$

These 18 forces will do work such that

$$\rho \frac{\partial E}{\partial t} = \left(\sigma_{ij}\, u_i\right)_{i,j}$$

or

$$M_{(L)} \frac{\partial}{\partial t} \left[I_{(L)} + \frac{1}{2} \left[u^2_{(L)} + v^2_{(L)} + w^2_{(L)}\right]\right]$$

$$= \{F11R(UR) + F11L(ULL) + F21T(UA) + F21B(UB)$$

$$+ F31F(UF) + F31B(UBA) + F22T(VA)$$

$$+ F22B(VB) + F12R(VR) + F12L(VLL)$$

$$+ F32F(VF) + F32B(VBA) + F33F(WF)$$

$$+ F33B(WBA) + F13R(WR) + F13L(WLL)$$

$$+ F23T(WA) + F23B(WB)\} = \Delta E$$

or

$$\Delta Q_{(L)} = \frac{\Delta t}{M_{(L)}}(\Delta E) - \left[u_{(L)} \Delta u_{(L)} + v_{(L)} \Delta v_{(L)} + w_{(L)} \Delta w_{(L)}\right.$$

$$\left. + \frac{\Delta u_{(L)}^2 + \Delta v_{(L)}^2 + \Delta w_{(L)}^2}{2}\right]$$

where the u, v and w are Phase 1 velocities and the velocity multiplying the stress is an average velocity (Phase 1) across that particular face at which the stress is applied. This requires the saving of columns and slabs of u, v and w velocities from Phase 1.

One requires only to solve for the stresses at the top, right and front of each cell, since the stresses have been calculated at the bottom (from the previous row), at the left (from the previous column sweep) and at the back (from the previous slab sweep).

The stresses at the right (R) side of the cell (see the figure below) are

$$\sigma_{ij} = B\left(\dot{e}_{ij} - \frac{\delta_{ij}}{3}\dot{e}_{aa}\right)$$

where

$$B = \left(\frac{2y^2}{\dot{\varepsilon}_{ab}\,\dot{\varepsilon}_{ab}}\right)^{1/2}$$

(y is defined on page 22)

On the right side (R), the stresses are

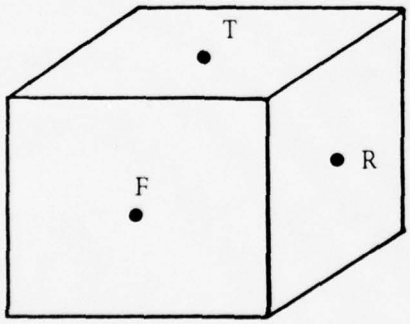

$$S11R = BR\left[\frac{\partial u}{\partial x} - \frac{1}{3}\left(\frac{\partial u}{\partial x} + \frac{\partial v}{\partial y} + \frac{\partial w}{\partial z}\right)\right]$$

$$S12R = \frac{BR}{2}\left[\frac{\partial u}{\partial y} + \frac{\partial v}{\partial x}\right]$$

$$S13R = \frac{BR}{2}\left[\frac{\partial u}{\partial z} + \frac{\partial w}{\partial x}\right]$$

On the top side (T), the stresses are

$$S22T = BT\left[\frac{\partial v}{\partial y} - \frac{1}{3}\left(\frac{\partial u}{\partial x} + \frac{\partial v}{\partial y} + \frac{\partial w}{\partial z}\right)\right]_J$$

$$S21T = \frac{BT}{2}\left[\frac{\partial v}{\partial x} + \frac{\partial u}{\partial y}\right]$$

$$S23T = \frac{BT}{2}\left[\frac{\partial v}{\partial z} + \frac{\partial w}{\partial y}\right]$$

On the front side (F), the stresses are

$$S33F = BF\left[\frac{\partial w}{\partial z} - \frac{1}{3}\left(\frac{\partial u}{\partial x} + \frac{\partial v}{\partial y} + \frac{\partial w}{\partial z}\right)\right]$$

$$S32F = \frac{BF}{2}\left[\frac{\partial w}{\partial y} + \frac{\partial v}{\partial z}\right]$$

$$S31F = \frac{BF}{2}\left[\frac{\partial w}{\partial x} + \frac{\partial u}{\partial z}\right]$$

The velocity gradients and the second strain rate tensor $\dot{\varepsilon}_{ab}$ $\dot{\varepsilon}_{ab}$ are all calculated at the three positions indicated and the velocities are the tilda (~) Phase 1 velocities.

Provisions exist for subcycling this strength routine. The Δt for each subcycle is not $\Delta t_H/N$ (where Δt_H is the hydrodynamic time step) but is calculated as follows:

$$\Delta t_H \frac{(N2+1-N)2}{N2(N2+1)}$$

where N2 = number of subcycles and N is the particular subcycle.

The yield strength in simple shear is considered to be a function of pressure and energy and is calculated as

$$Y = (Y_0 + \alpha P)(1 - Q/Q_M)$$

where

Y_0 = yield strength, jerks/cm^3

α = constant

Q_M = energy to melt, jerks/g .

The rigid plastic equations are only applied to those zones that have a $\rho/\rho_0 > 1.0$ or if $\rho/\rho_0 < 1.0$ and $Q > Q_I$ (Q_I is an input number).

Those cells, in which the original velocity has not changed by ∿5%, are bypassed for the strength calculation (Phase 3).

III. TWO THREE-DIMENSIONAL IMPACT CALCULATIONS

A comparison between a normal (two-dimensional R-Z) calculation and a normal (x-y-z) calculation has been completed for a normal impact.

An infinite copper jet moving at a velocity of 7.5×10^5 cm/sec impacted an aluminum target of finite thickness. The radius of the jet (for the two-dimensional calculation) was .115 cm, and keeping the same cross-sectional area for the projectile, resulted in a square cross-sectional rod of .204 cm on each side (Figure III-1).

The Tillotson form of the equation of state was used both in DORF and TRIDORF. The two-dimensional calculation was performed using a grid of 45 zones in the radial, and 48 zones in the axial direction. The three-dimensional calculation was performed using a grid of 12 zones in the x direction, 23 zones in the y direction and 12 zones in the z direction. Note, it is only necessary to solve one-fourth of the problem in the three-dimensional mode, because of the two planes of symmetry.

The results are shown (Figure III-2) for the pressure along the axis of symmetry for the two calculations at a time of about .54 μsec. The agreement is very good, considering the very coarse zoning in the three-dimensional grid. Results such as these add to the credibility of the TRIDORF code.

IV. OBLIQUE IMPACT

Two calculations, using TRIOIL (with strength), were completed several years ago for the Naval Research Laboratory. The configurations were as follows: A plexiglass sphere (R = .3175 cm) impacting at a velocity of 6.1×10^5 cm/sec on a thin plexiglass target of 2.54 cm thickness. The spherical projectile impacted normal (Figure IV-1) and at 45° to the target (Figure IV-2) where the angle is measured between the flight path and the target.

The figures shown are for the plane of symmetry as a function of time. The sequence begins at the upper left and continues downward. The problem (normal) was rezoned (as indicated on the t = 1.68 μsec figure).

A series of four oblique impacts have been performed using the TRIDORF code. The four calculations involved a copper jet (R = .1 cm) impacting a thin steel target of 1.27 cm thickness. The copper jet was treated as a copper rod with a rectangular cross section (.1772 cm on each side). The impact velocity in all cases was chosen as 7.55×10^5 cm/sec.

Massless tracer particles were placed in an orthogonal grid within the steel plate and copper rod. The configurations at various times and for various planes are shown in Figures IV-3, IV-4, IV-5 and IV-6.

Figure IV-3 is a display of the interaction for the 30° impact problem. The cross-sectional display begins in the upper left, proceeding downwards, for the Z planes (coming out of the paper). The jaggedness of the top surface of the target is due to the large zones used in the calculation. Fine zones were placed in all three directions near the original target-projectile interface.

Figure IV-4 is a similar display for the 45° interaction. Figure IV-5 displays, in addition to the Z values, the interaction (plane of symmetry) as a function of time. The Z planes are displayed for every other Z value. These results are for the 60° impact.

Figure IV-6 is a similar display for the 77.5° impact, as a function of the Z planes. This calculation will require considerably more computer time for complete penetration (if complete penetration will occur).

V. FUEL TARGET INTERACTION

The problem of a copper jet traveling at a velocity of 5.617×10^5 cm/sec penetrating a cylindrical tank of fuel (initial density = 1 g/cc) has been completed. A modified continuous boundary condition at the bottom of the tank allowed the copper jet to continue through the tank at a constant velocity. The copper jet was treated as a rigid body, while the fuel was treated as compressible, using an

equation of state developed by John Dienes[5]. The form of the equation of state is

$$P = A\phi + B\phi^3 \quad , \quad \text{where } \phi = \log(\rho/\rho_0) \quad .$$

The calculation (two-dimensional) was carried to a time of $t = 1.84\mu$sec when the copper jet had penetrated the top of the cylindrical tank. Stress waves have reflected from the top of the tank, but the stress wave has not reached the upper right corner of the tank at this time.

Subroutines ADJUST and CUBIT were used to rezone the two-dimensional grid such that the axial and radial zoning will be identical to the x and y zoning for the three-dimensional problem. Figure V-1 indicates the initial configurations for the two- and three-dimensional problems. The radial pressure at the bottom of the cylindrical tank is displayed in Figure V-2B. The axial pressures (for given radial positions) are displayed in Figure V-2A. These results are at the completion of the two-dimensional calculation.

Figure V-3A shows density profiles for an early time (2-D) interaction. One can see the cavitation appearing along the rigid rod.

Representative pressures (at the completion of the three-dimensional calculation) are shown in Figures V-3B and V-3C. Figure V-3B shows pressure contours for the front face of the three-dimensional configuration. Figure V-3C shows the pressure contour for the bottom face of the box. Figure V-4A presents pressure versus distance along the bottom and top edge of the front face of the cube. Figure V-4B presents pressure versus time at the top right hand corner and bottom right hand corner of the front edge of the box. Additional pressure and velocity profiles are necessary to complete the flow patterns in the corners of the box.

---

[5] Dienes, John, "The Response of Gelatin to High Speed Impact, SSS-IR-74-2120.

VI. MULTI-MATERIAL IMPACT

The configuration for the multi-material impact is shown in Figure VI-1.

A copper jet (R = 1 mm) impacted on a finite aluminum target (thickness of 3.75 cm) at a velocity of 7.5×10^5 cm/sec. There are 35 zones in the radial direction and 90 zones in the axial direction.

Figure VI-2 shows density plots of the interaction as a function of time. The density plots are produced by assigning $\sim$100 random particles to the cell with the largest density. All other cells are then plotted with a number of particles proportional to the cell density divided by the maximum density multiplied by 100.

VII. CODE MODIFICATIONS

Several code modifications were required in order to complete the fuel target interaction problem.

The slug was treated as a rigid body and moved through the grid with a constant velocity. This required modifications in the transport phase and the Lagrangian phase of the DORF code. A continuous bottom boundary condition was required in order to simulate the infinite slug. An artificial viscosity routine (with linear and quadratic terms) was incorporated into the DORF code. The viscosity is calculated at the zone interfaces rather than cell centers. These artificial viscosity terms were then incorporated into the momentum and energy equations for the Lagrangian phase of the calculation.

The two-dimensional calculation for the slug penetration was carried out until the stress wave reached the wall. At this time, the codes ADJUST[3] and CUBIT[3] were used to rezone the problem such that the zoning in the R and Z direction for the two-dimensional results would be identical to the zoning in the X and Y direction for a plane in the three-dimensional grid. One can then transfer the v component of velocity, the specific internal energy and the density directly and transform the u component of velocity from the two-dimensional grid to the u and w components in the three-dimensional grid.

Modifications to the DORF code for interior rigid boundaries have been completed. These interior boundaries must coincide with cell boundaries. A material flag, "9", designates that the 4 sides of the cell are to be treated as reflective boundaries. Options of allowing the bottom, top and right side of the computational grid to be either reflective or transmittive have been added. The sound speed for the Tillotson formulation of the equation of state has been changed to perform the evaluation of the analytical form of

$$c^2 = \left.\frac{\partial P}{\partial \rho}\right|_Q + \left.\frac{\partial P}{\partial Q}\right|_\rho \frac{P}{\rho^2} \quad .$$

Basic equations for a splitting version of the OIL code have been derived. In addition, the conventional "if" tests have been removed and replaced with functions whose values are 0 or 1.0. The splitting technique and the removal of the conventional "if" tests are applicable to the new generation of parallel and vector computers.

ACKNOWLEDGMENTS

Motivation and direction were given by Dr. Val Kucher and Dr. John Majerus of the Ballistics Research Laboratories, for which the author is indeed grateful.

The author is also very grateful for the support of James Tabor of the Los Alamos Scientific Laboratory for the color slides depicting the results of the three-dimensional calculations.

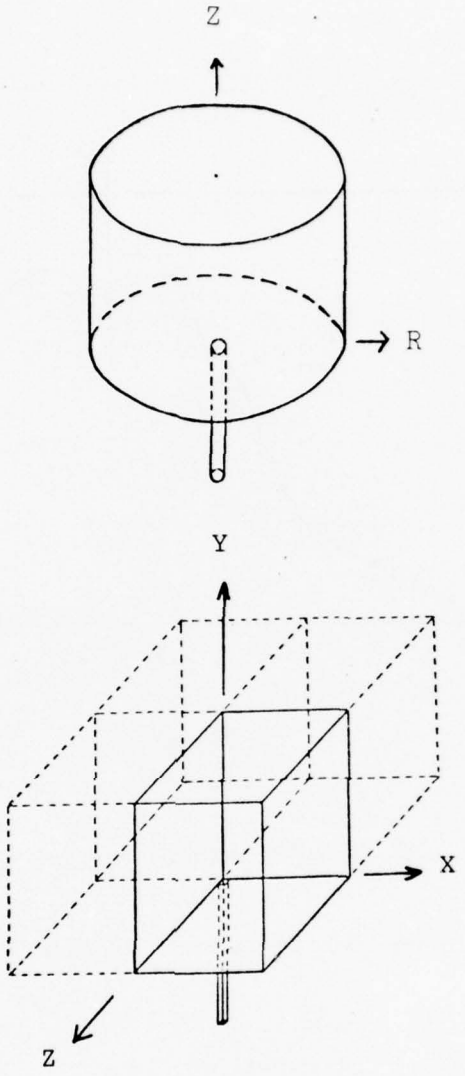

Figure III-1. 2D - 3D Initial Configuration for Normal Impact

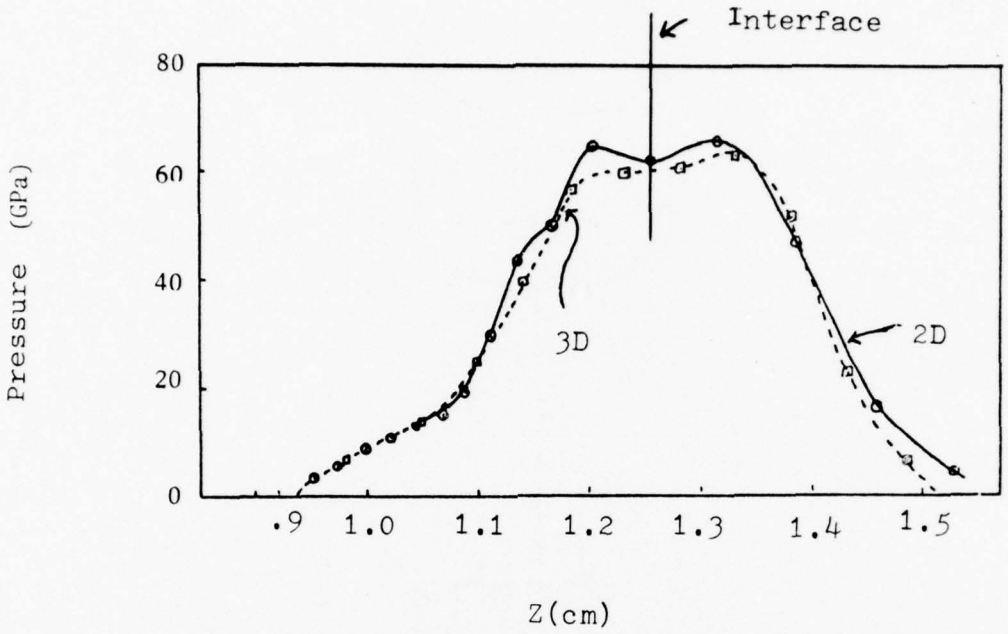

3D t=.528 μsec cycle=72

2D t=.54 μ sec cycle=70

Figure III-2. Pressure Versus Distance (into Target) for 2D - 3D

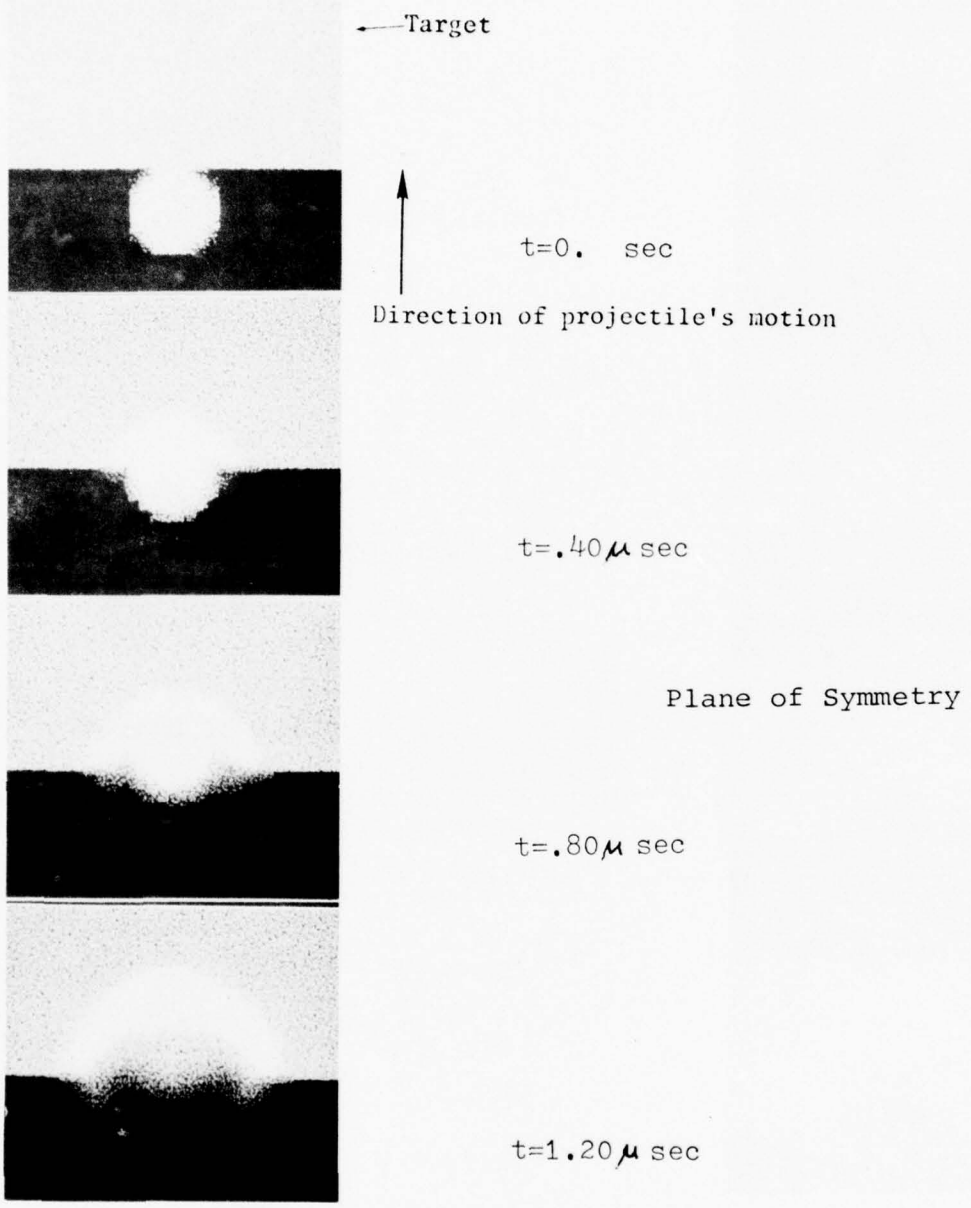

Figure IV-1. Density as a Function of Time for the Normal Impact

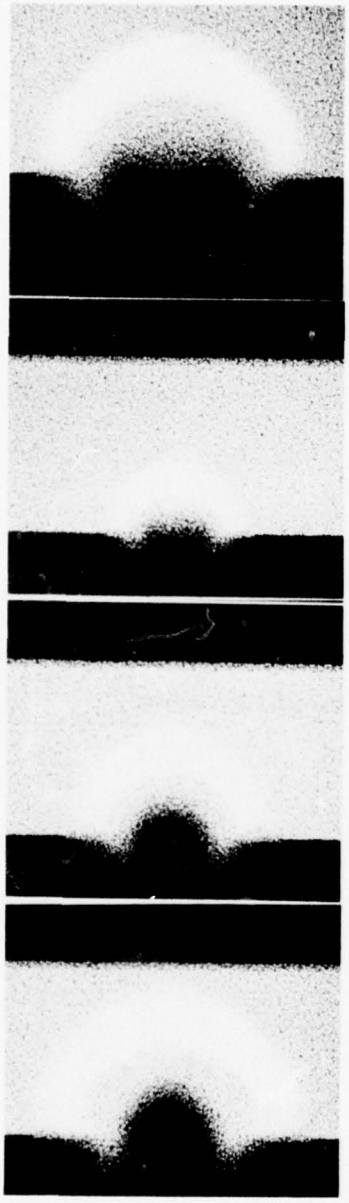

Figure IV-1. Density as a Function of Time for the Normal Impact (continued)

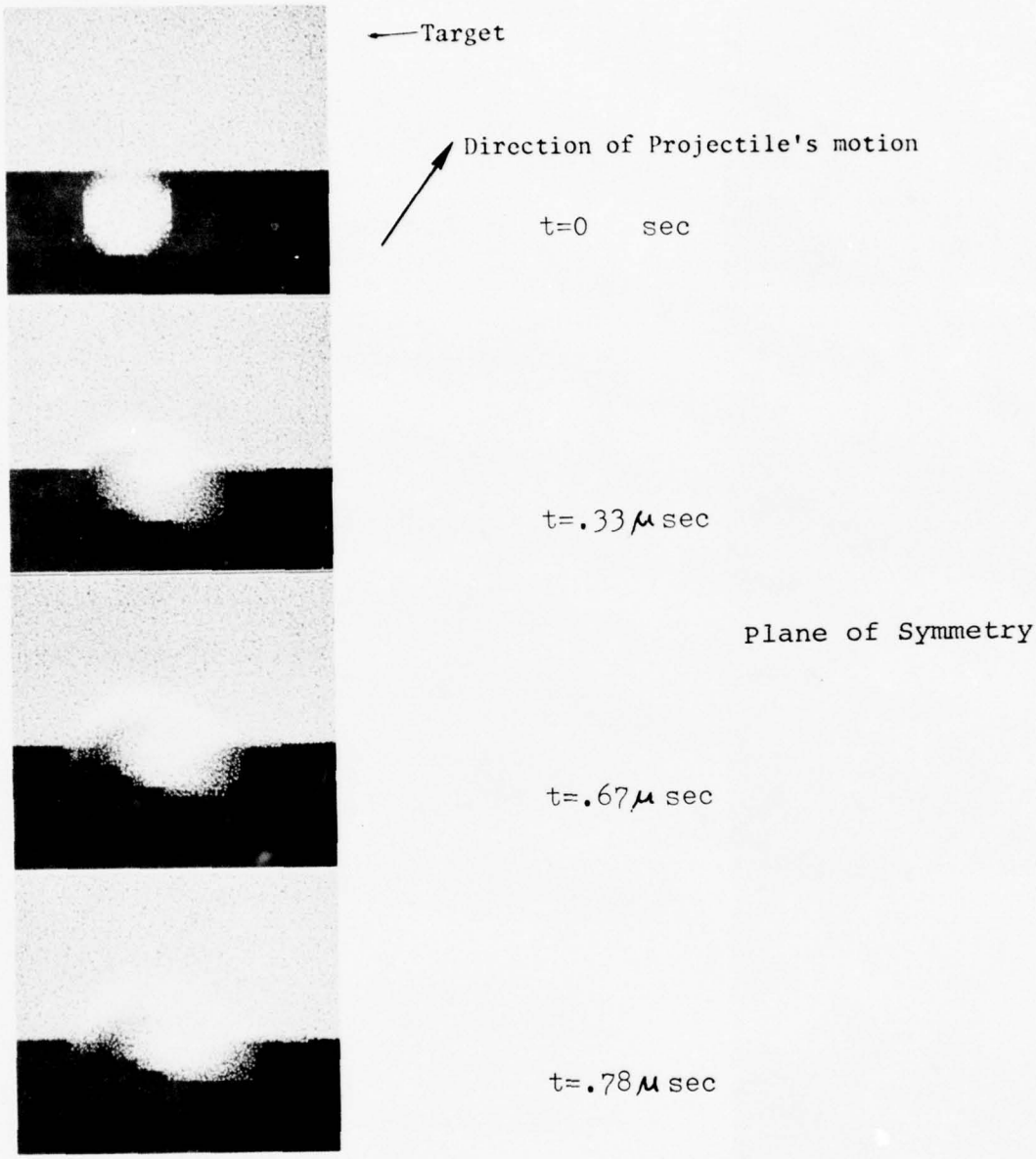

Figure IV-2. Density as a Function of Time for the 45° Impact

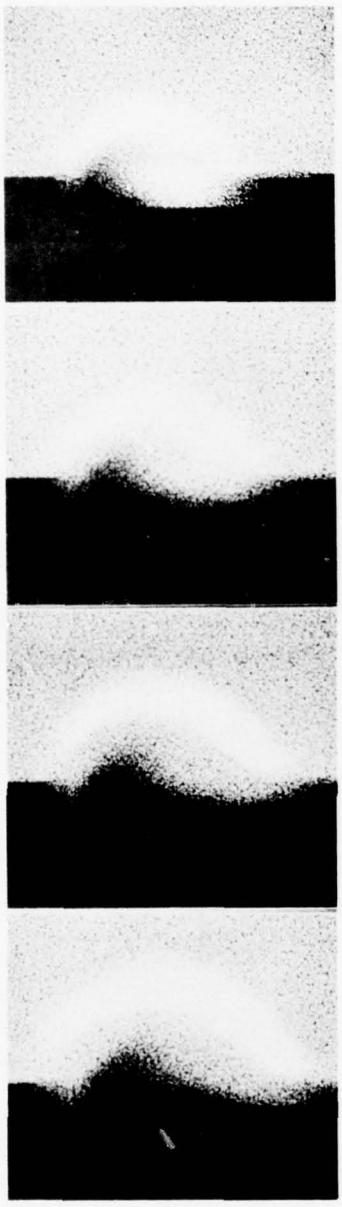

t=.90μ sec

t=1.15μ sec

Plane of Symmetry

t=1.40μ sec

t=1.7μ sec

Figure IV-2. Density as a Function of Time for the 45° Impact (continued)

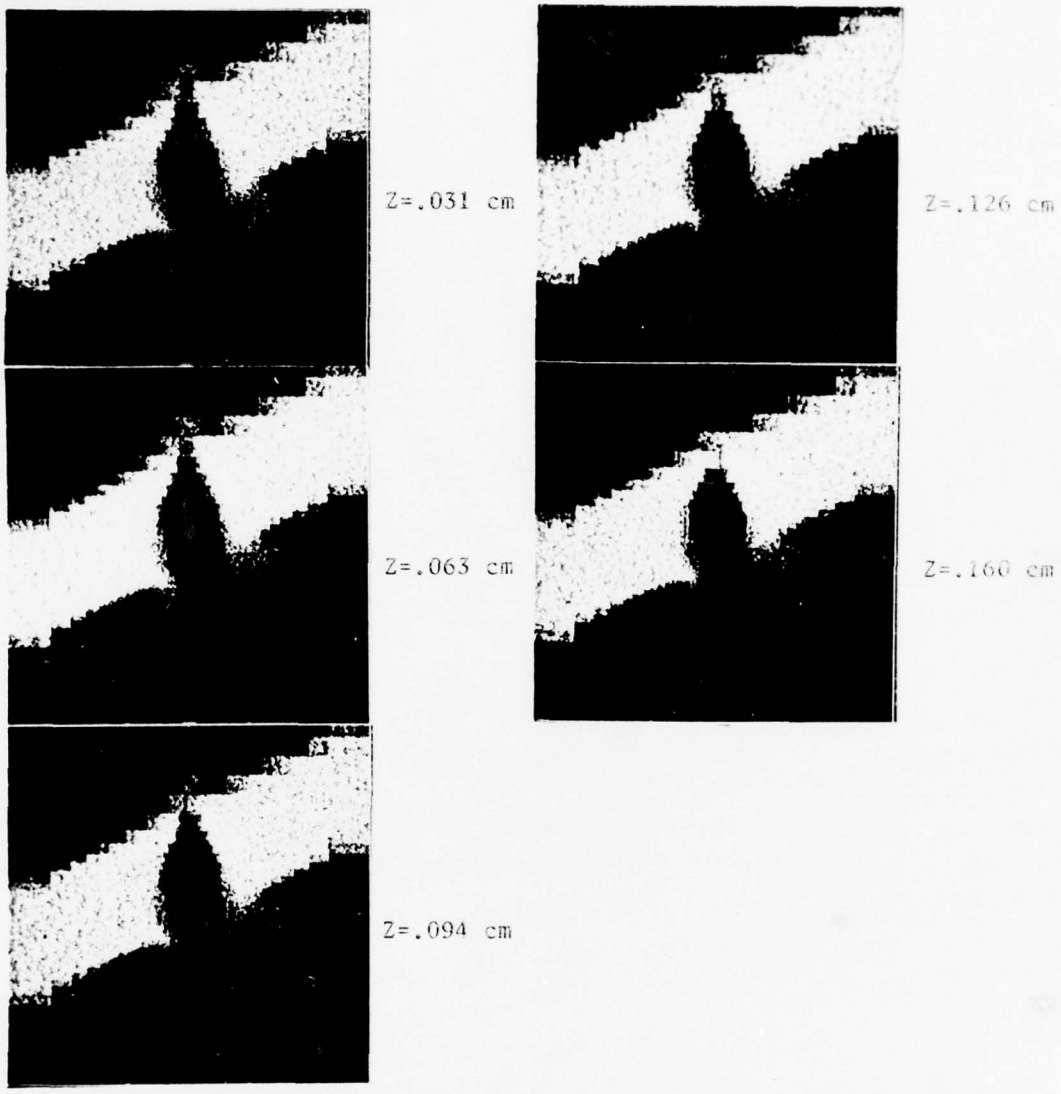

Figure IV-3. Density as a Function of Z at a Time of 3.57 μsec for the 30° Impact

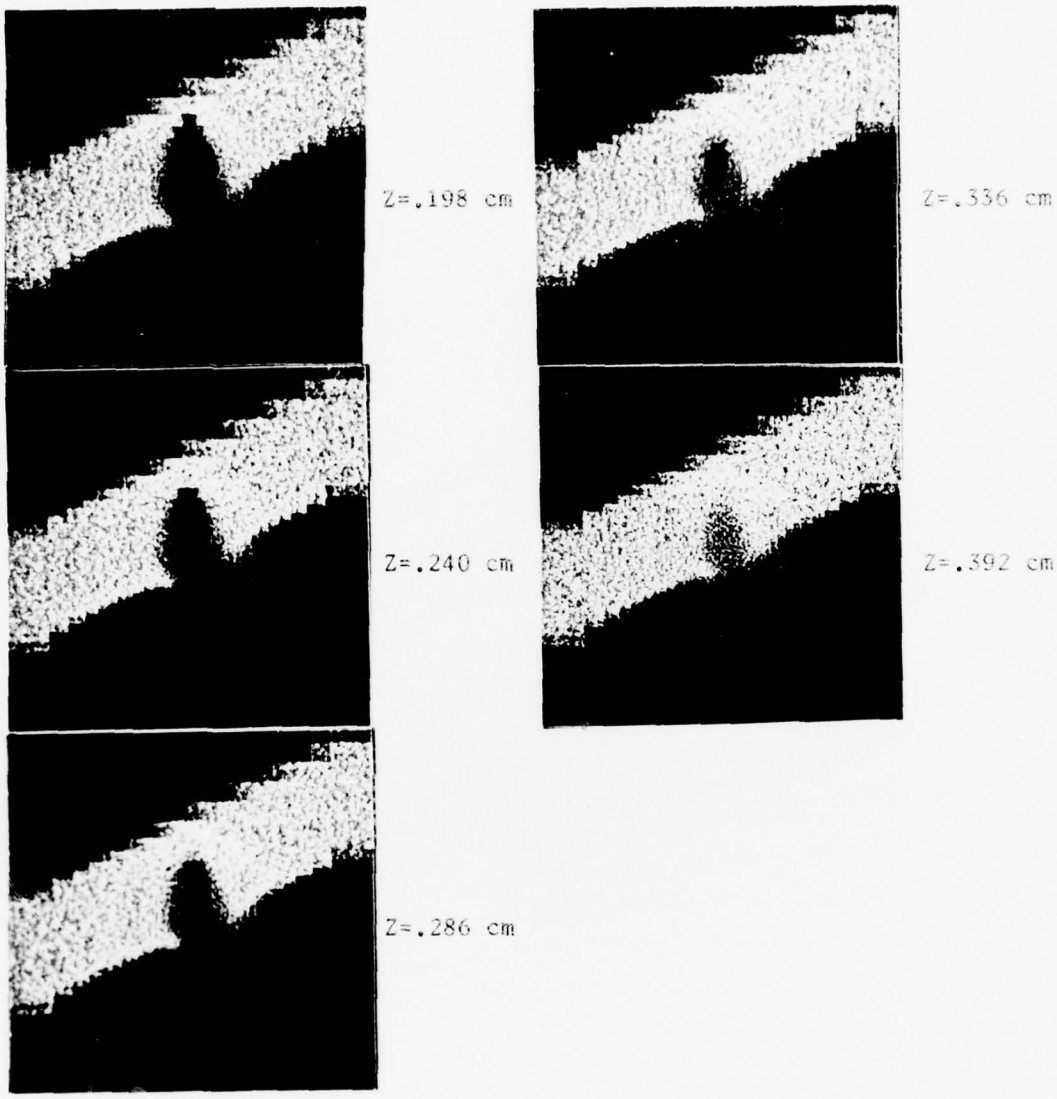

Figure IV-3. Density as a Function of Z at a Time of 3.57 usec for the 30° Impact (continued)

PRECEDING PAGE BLANK-NOT FILMED

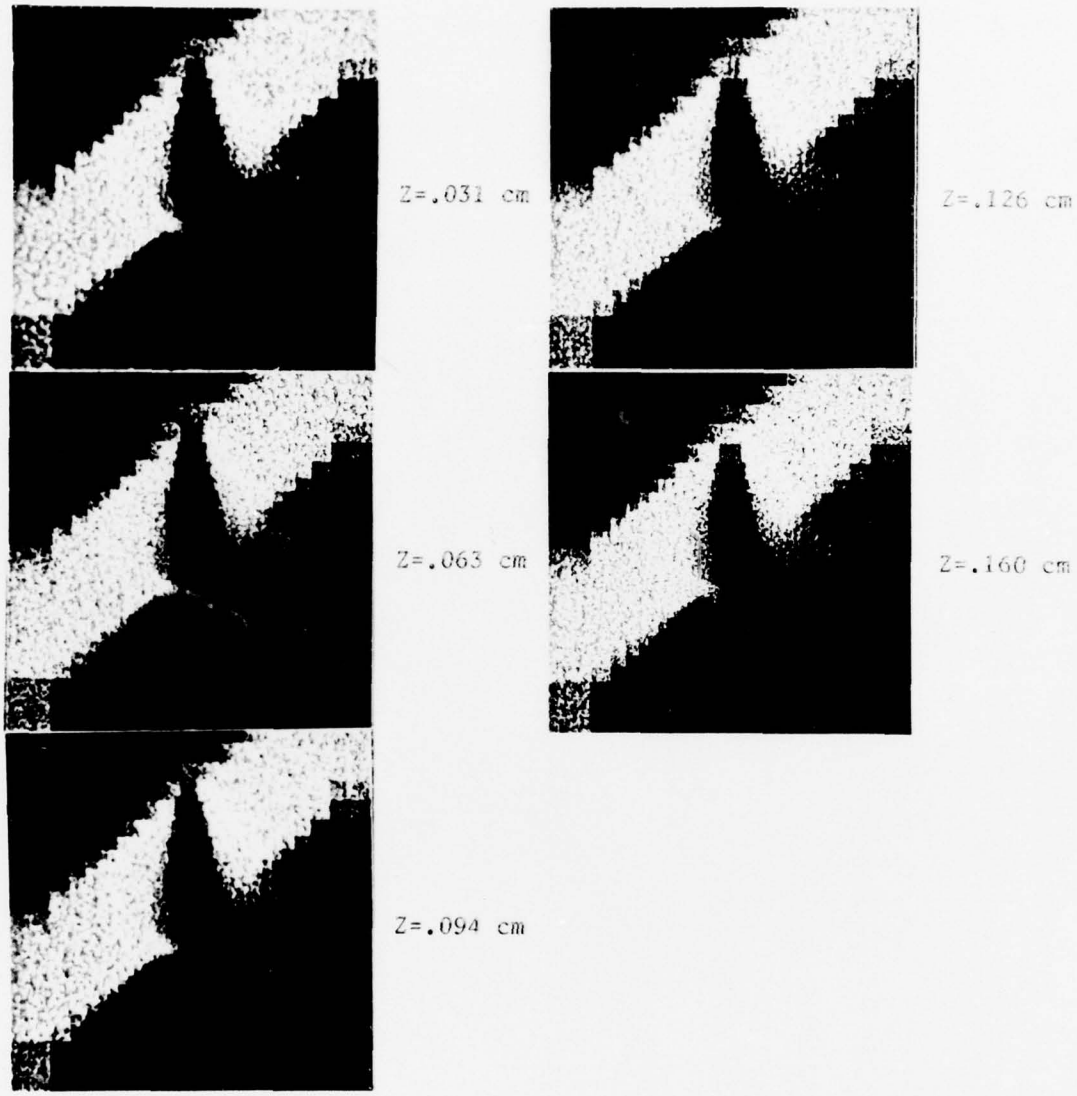

Figure IV-4. Density as a Function of Z at a Time of 4.41 μsec for the 45° Impact

PRECEDING PAGE BLANK-NOT FILMED

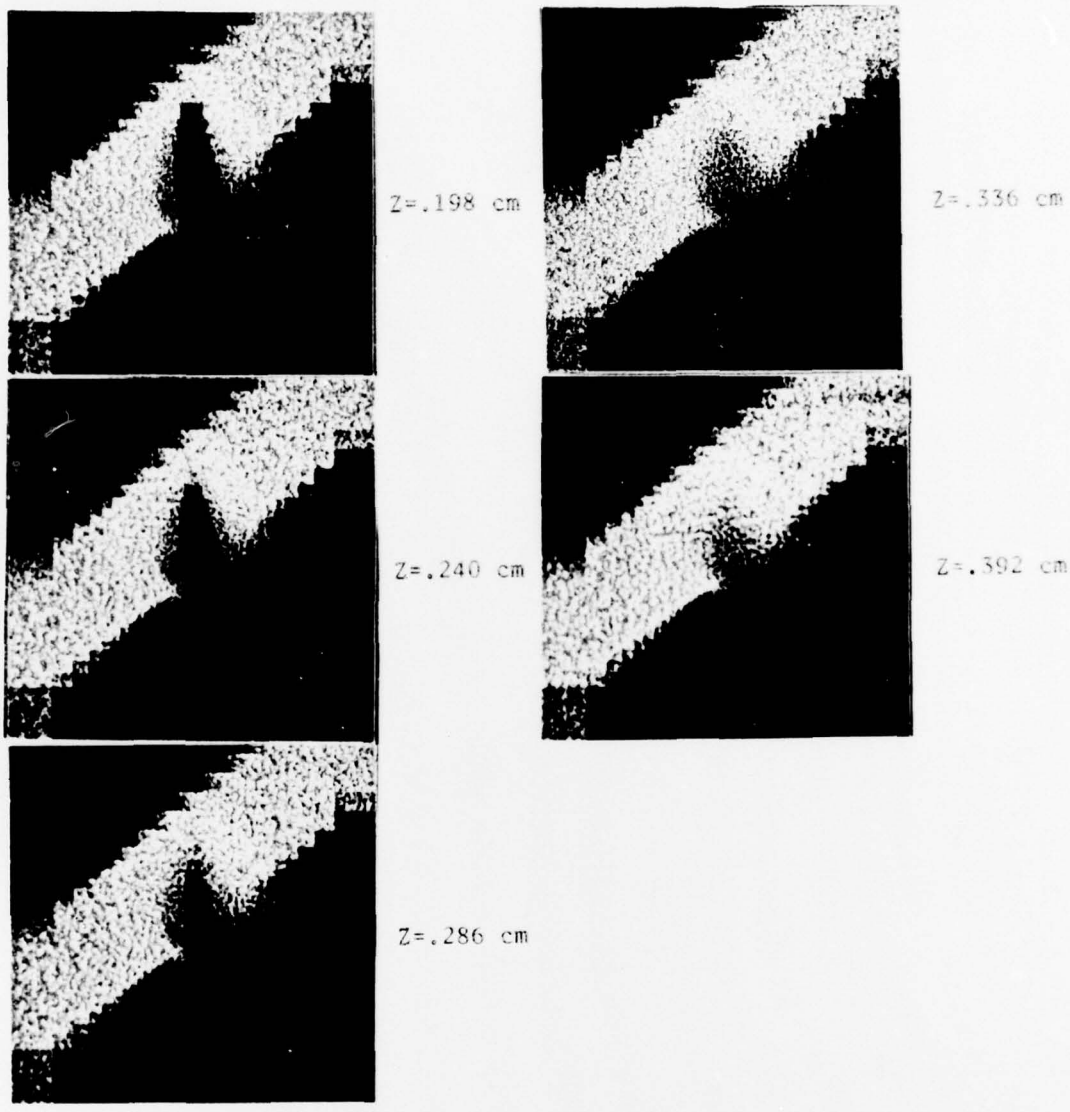

Figure IV-4. Density as a Function of Z at a Time of 4.41 μsec for the 45° Impact (continued)

PRECEDING PAGE BLANK-NOT FILMED

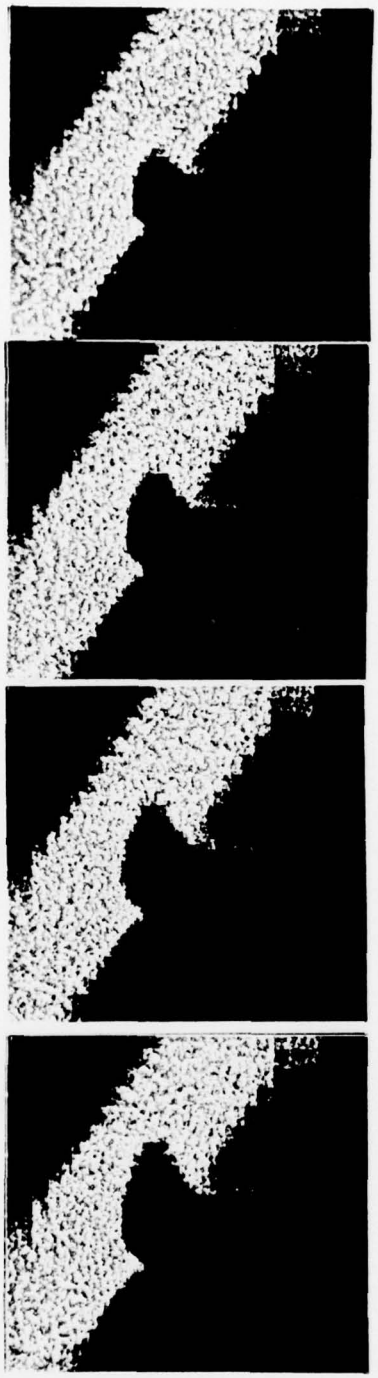

Figure IV-5. Density as a Function of Time and Z for the 60° Impact

PRECEDING PAGE BLANK-NOT FILMED

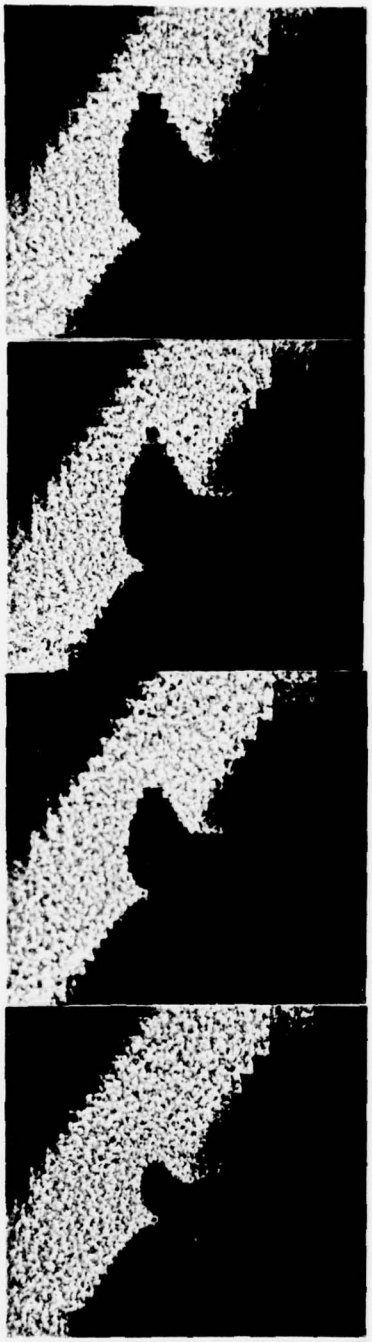

Figure IV-5. Density as a Function of Time and Z for the 60° Impact (continued)

PRECEDING PAGE BLANK-NOT FILMED

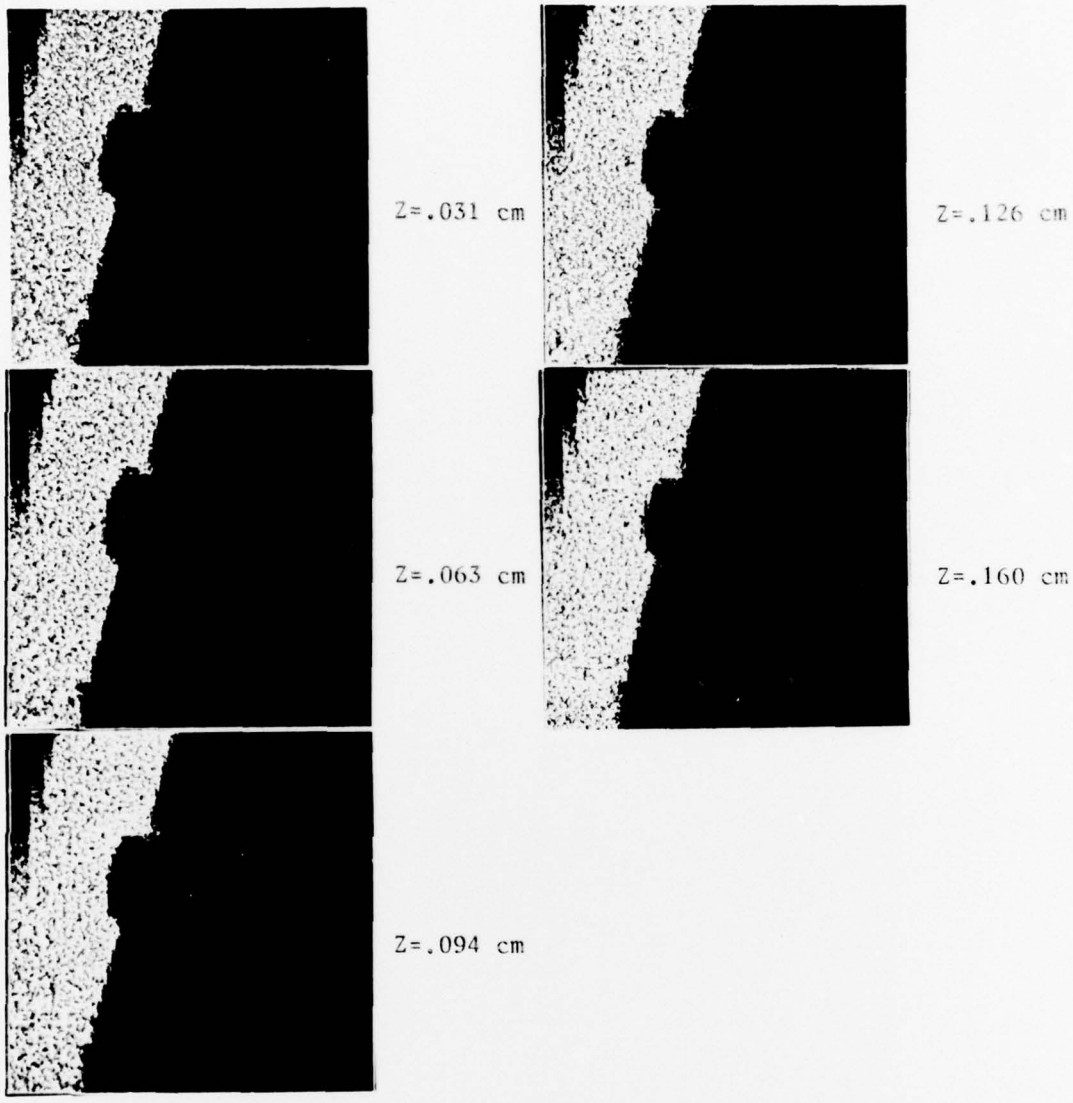

t=2.67 μsec

Figure IV-6. Density as a Function of Z for the 77.5° Impact

PRECEDING PAGE BLANK-NOT FILMED

t=2.67 μsec

Figure IV-6. Density as a Function of Z for the 77.5° Impact (continued)

PRECEDING PAGE BLANK-NOT FILMED

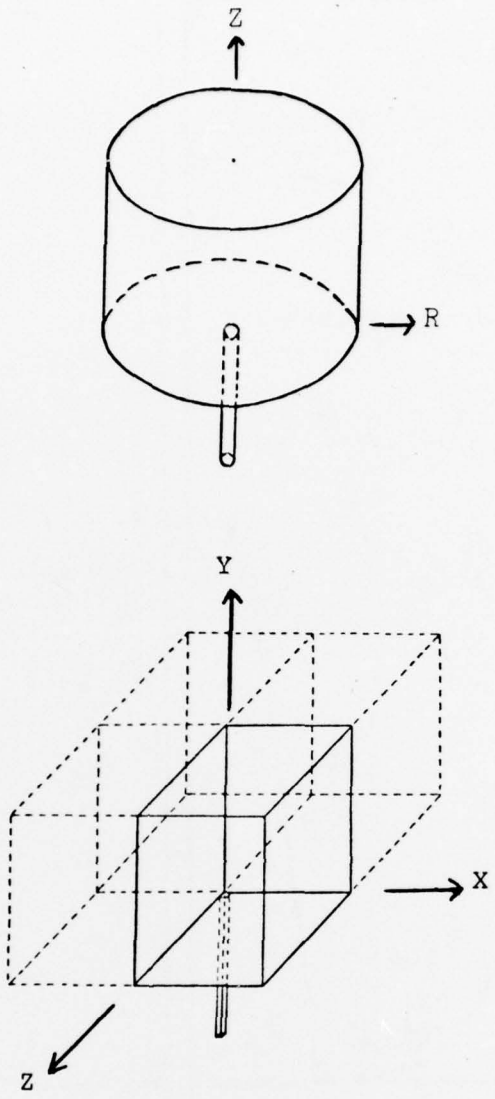

Figure V-1. Initial Fuel Target Interaction (2D - 3D)

PRECEDING PAGE BLANK-NOT FILMED

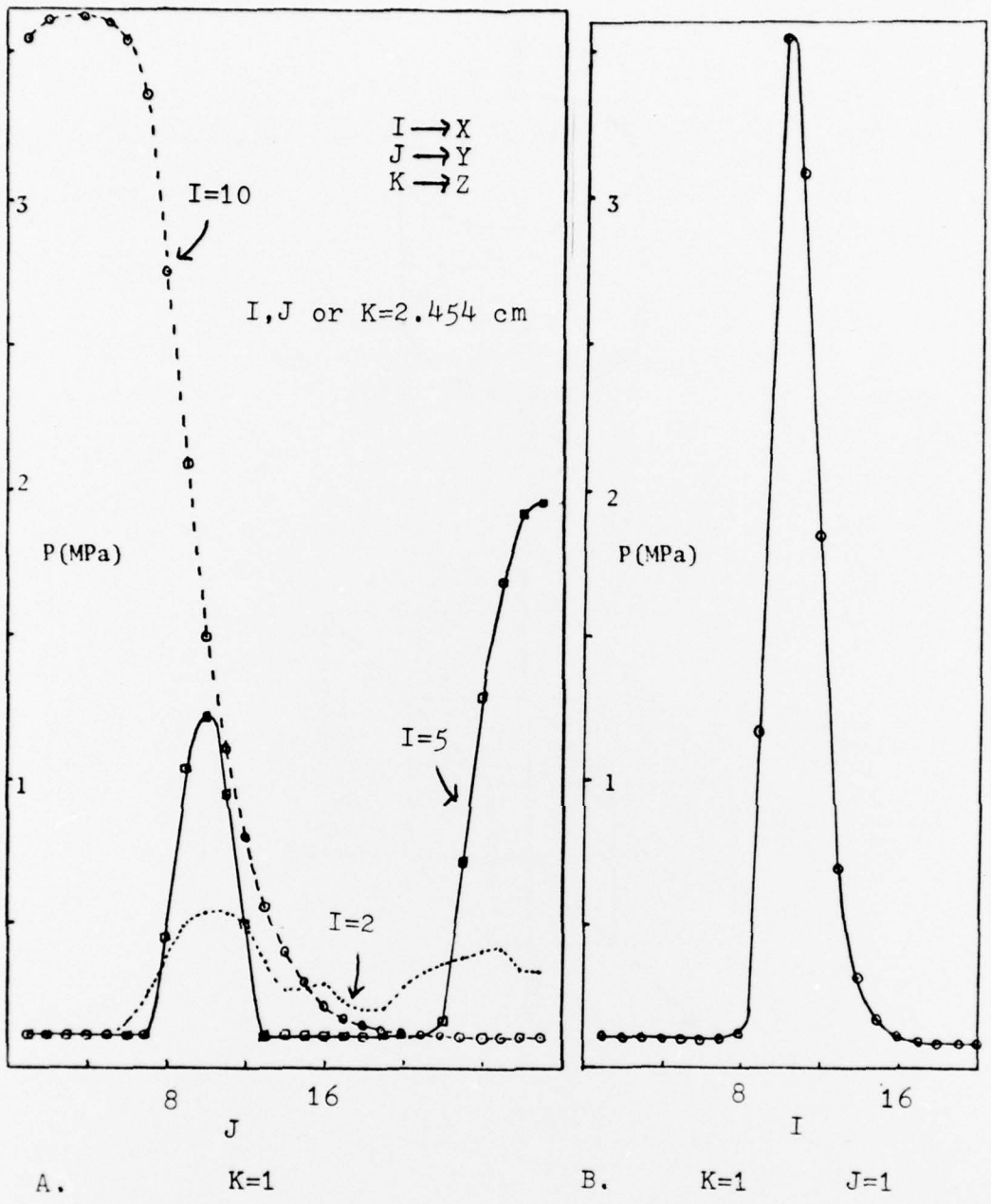

Figure V-2. Pressures in 3D Mesh at Time of Rezone

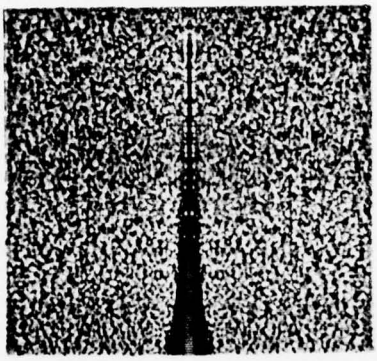

A. Early Time Density Distribution (2D)

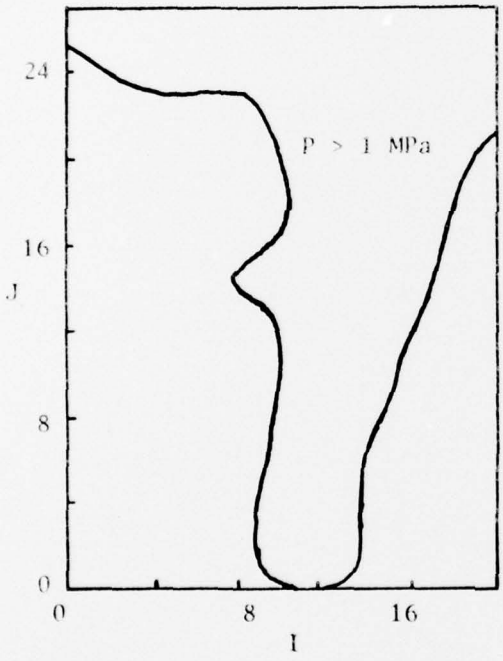

B. Front (K=20)

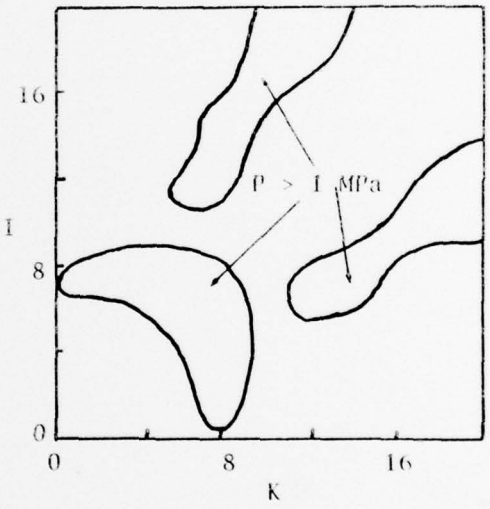

C. Bottom (J=1)

Figure V-3. Pressure Contours at Completion of 3D Calculations

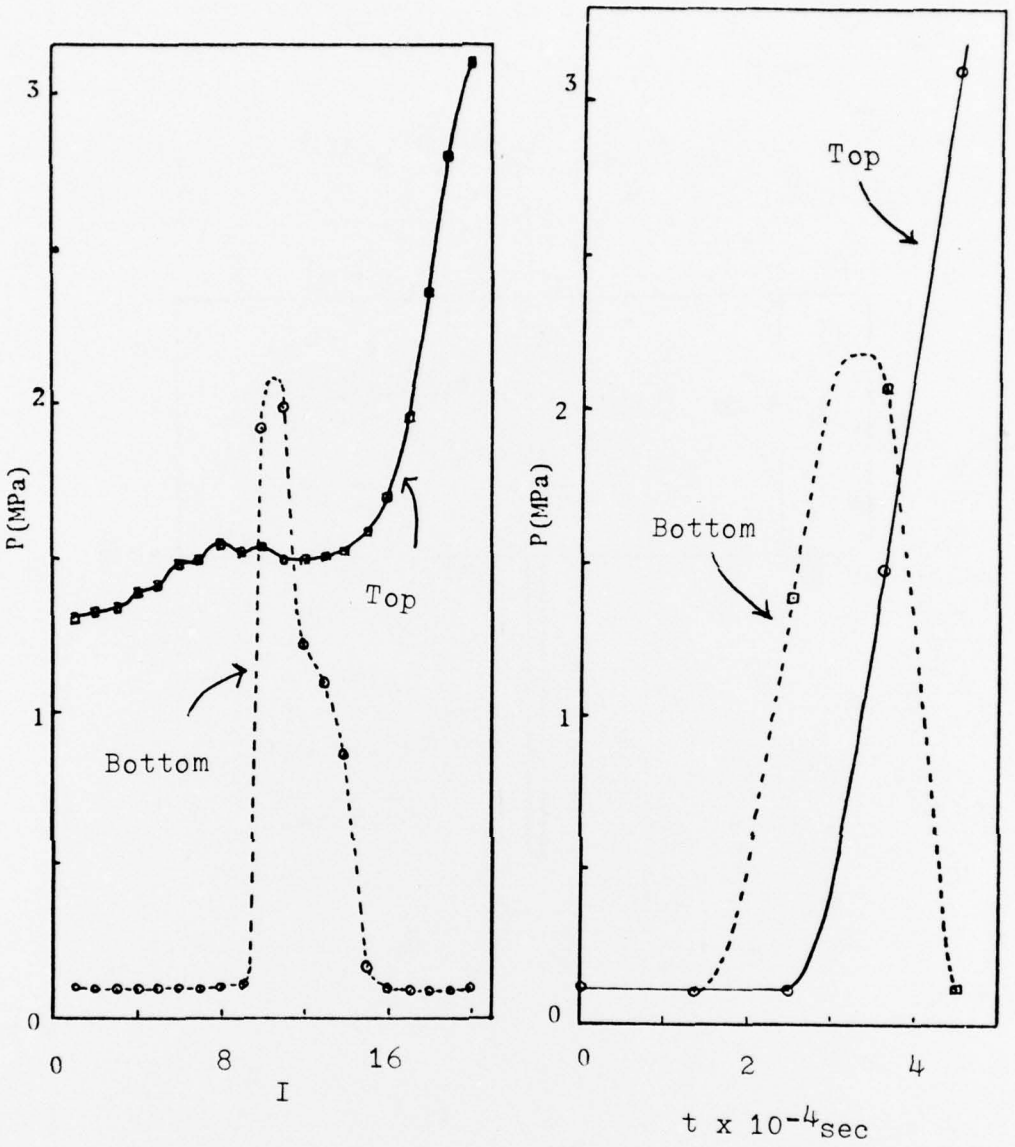

A. K=20

B. Top and Bottom (right corner) for K=20

Figure V-4. Pressure Distribution at Completion of 3D Calculation

PRECEDING PAGE BLANK-NOT FILMED

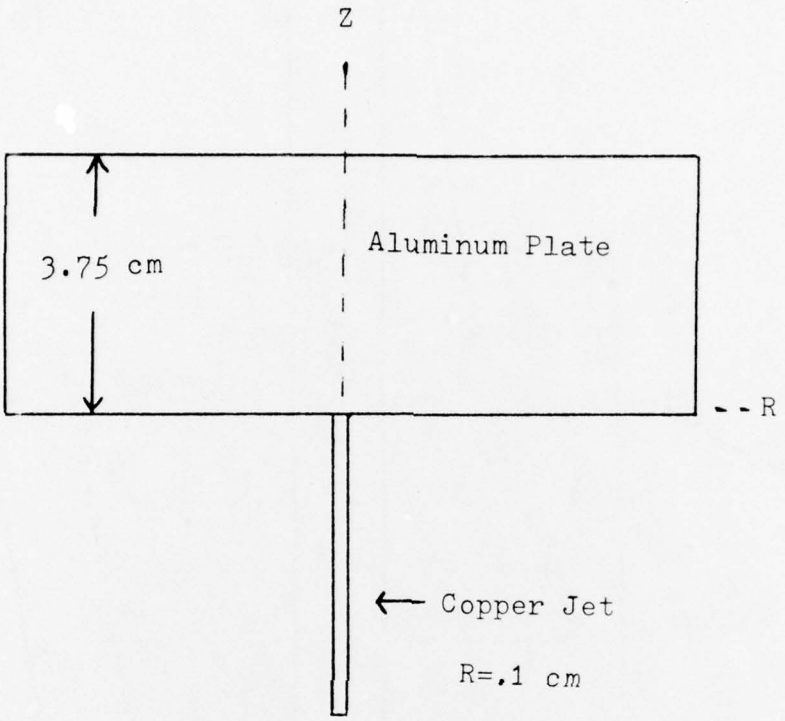

Figure VI-1. Initial Configuration for the Multi-Material Normal Impact

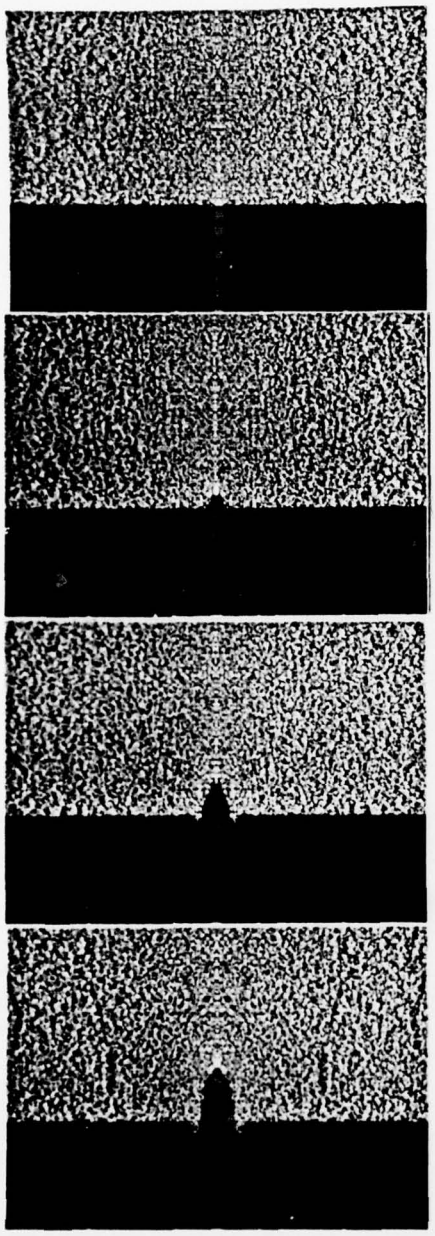

Figure VI-2. Density as a Function of Time for the Multi-Material Normal Impact

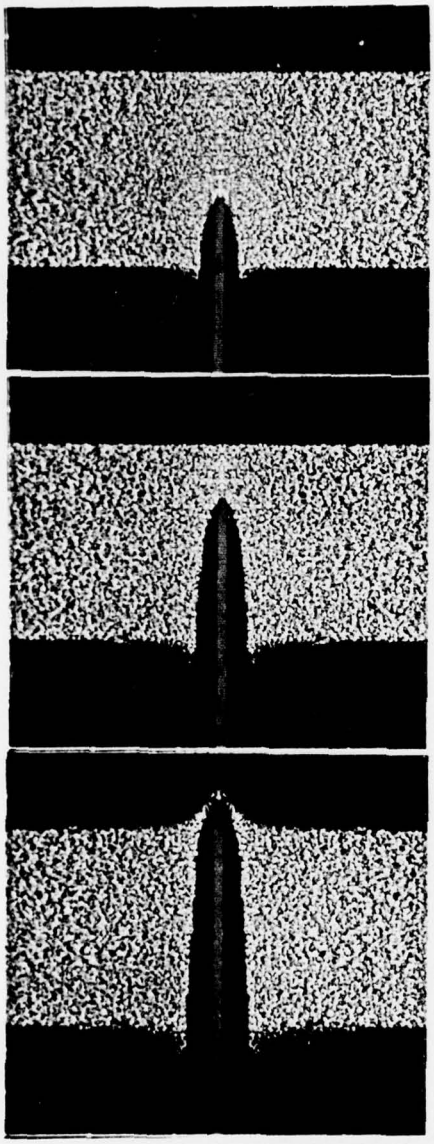

t=2.84 μsec

t=5.69 μsec

t=8.85 μsec

Figure VI-2. Density as a Function of Time for the Multi-Material Normal Impact (continued)

PRECEDING PAGE BLANK-NOT FILMED

DISTRIBUTION LIST

No. of Copies	Organization
12	Commander Defense Documentation Center ATTN: DDC-TCA Cameron Station Alexandria, VA 22314
1	Commander US Army Materiel Development and Readiness Command ATTN: DRCDMA-ST 5001 Eisenhower Avenue Alexandria, VA 22333
1	Commander US Army Aviation Systems Command ATTN: DRSAV-E 12th and Spruce Streets St. Louis, MO 63166
1	Director US Army Air Mobility Research and Development Laboratory Ames Research Center Moffett Field, CA 94035
1	Commander US Army Electronics Command ATTN: DRSEL-RD Fort Monmouth, NJ 07703
1	Commander US Army Missile Research and Development Command ATTN: DRDMI-R Redstone Arsenal, AL 35809
1	Commander US Army Tank Automotive Development Command ATTN: DRDTA-RWL Warren, MI 48090
2	Commander US Army Mobility Equipment Research & Development Command ATTN: Tech Docu Cen, Bldg. 315 DRSME-RZT Fort Belvoir, VA 22060
1	Commander US Army Armament Materiel Readiness Command Rock Island, IL 61202
2	Commander US Army Armament Research and Development Command ATTN: J. Pearson Tech Lib Dover, NJ 07801
1	Commander US Army Harry Diamond Labs ATTN: DRXDO-TI 2800 Powder Mill Road Adelphi, MD 20783
1	Commander US Army Materials and Mechanics Research Center ATTN: Tech Lib Watertown, MA 02172
1	Director US Army TRADOC Systems Analysis Activity ATTN: ATAA-SA White Sands Missile Range NM 88002
1	Assistant Secretary of the Army (R&D) ATTN: Asst for Research Washington, DC 20310

PRECEDING PAGE BLANK-NOT FILMED

DISTRIBUTION LIST

No. of Copies	Organization
1	Commander US Army Research Office P. O. Box 12211 Research Triangle Park NC 27709
1	Chief of Naval Research Department of the Navy Washington, DC 20325
1	Commander US Naval Ordnance Systems Cmd ATTN: Code ORD-0332 Washington, DC 20360
1	Commander US Naval Surface Weapons Center ATTN: Tech Lib Dahlgren, VA 22448
2	Commander US Naval Surface Weapons Center ATTN: Code 730 Lib Silver Spring, MD 20910
1	Commander US Naval Weapons Center ATTN: Code 45, Tech Lib China Lake, CA 93555
1	Commander US Naval Research Laboratory Washington, DC 20375
1	US Air Force Academy ATTN: Code FJS-RL (NC) Tech Lib Colorado Springs, CO 80840
1	AFAL (AVW) Wright-Patterson AFB, OH 45433
1	AFLC (MMWMC) Wright-Patterson AFB, OH 45433
1	Director Lawrence Radiation Laboratory ATTN: Mr. M. Wilkins P. O. Box 808 Livermore, CA 94550
1	Director National Aeronautics and Space Administration Langley Research Center Langley Station Hampton, VA 23365
1	Computer Code Consultants ATTN: Mr. W. Johnson 527 Glencrest Drive Solana Beach, CA 92075
1	Sandia Laboratories ATTN: L. Bertholf Albuquerque, NM 87115
1	Systems, Science & Software ATTN: Dr. R. Sedgwick P. O. Box 1620 La Jolla, CA 92037
1	Drexel Institute of Technology Wave Propagation Research Center ATTN: Prof. P. Chou 32nd & Chestnut Streets Philadelphia, PA 19104
2	University of California Los Alamos Scientific Lab ATTN: Tech Lib Dr. J. M. Walsh P. O. 1663 Los Alamos, NM 87545
	Aberdeen Proving Ground
	Marine Corps Ln Ofc Dir, USAMSAA